Title : Genetic diversity of Collaborative Cross mice controls viral replication, clinical severity and brain pathology induced by Zika virus infection, independently of *Oas1b*.

Running title : Host genetic susceptibility to Zika virus disease

Caroline Manet,[a] Etienne Simon-Lorière,[b] Grégory Jouvion,[c,d] David Hardy,[c] Matthieu Prot,[b] Marie Flamand,[e] Jean-Jacques Panthier,[a] Anavaj Sakuntabhai,[f] Xavier Montagutelli[a#]

Affiliations:

[a]Mouse Genetics Laboratory, Institut Pasteur, Department of Genomes and Genetics, Institut Pasteur, 75015 Paris, France

[b] Evolutionary Genomics of RNA Viruses, Department of Virology, Institut Pasteur, CNRS UMR 3569, 75015 Paris, France

[c]Sorbonne Université, INSERM, Pathophysiology of Pediatric Genetic Diseases, AP-HP, Hôpital Armand-Trousseau, UF de Génétique Moléculaire, 75012 Paris, France

[d]Institut Pasteur, Experimental Neuropathology Unit, Department of Global Health, 75015 Paris, France

[e]Structural Virology Unit, Department of Virology, CNRS UMR 3569, Institut Pasteur, 75015 Paris, France

[f]Functional Genetics of Infectious Diseases Unit, Department of Global Health, Institut Pasteur, CNRS UMR 2000, 75015 Paris, France

#Address correspondence to Xavier Montagutelli, xavier.montagutelli@pasteur.fr

Word counts : Abstract : 225 - Text : 7982

ABSTRACT

The explosive spread of Zika virus (ZIKV) has been associated with major variations in severe disease and congenital afflictions among infected populations, suggesting an influence of host genes. We investigated how genome-wide variants could impact susceptibility to ZIKV infection in mice. We first describe that the susceptibility of *Ifnar1* knockout mice is largely influenced by their genetic background. We then show that the broad genetic diversity of Collaborative Cross mice, which receptor to type I interferon (IFNAR) was blocked by anti-IFNAR antibody, expressed phenotypes ranging from complete resistance to severe symptoms and death with large variations in the peak and rate of decrease of plasma viral load, in brain viral load, in brain histopathology and in viral replication rate in infected cells. Differences of susceptibility between CC strains were correlated between Zika, Dengue and West Nile viruses. We identified highly susceptible and resistant mouse strains as new models to investigate the mechanisms of human ZIKV disease and other flavivirus infections. Genetic analyses revealed that phenotypic variations are driven by multiple genes with small effects, reflecting the complexity of ZIKV disease susceptibility in human population. Notably, our results rule out a role of the *Oas1b* gene in the susceptibility to ZIKV. Altogether, this study emphasizes the role of host genes in the pathogeny of ZIKV infection and lays the foundation for further genetic and mechanistic studies.

IMPORTANCE

In recent outbreaks, ZIKV has infected millions of people and induced rare but potentially severe complications, including Guillain-Barré syndrome and encephalitis in adults. While several viral sequence variants were proposed to enhance the pathogenicity of ZIKV, the influence of host

23   genetic variants in the clinical heterogeneity remains mostly unexplored. We have addressed this

24   question using a mouse panel which models the genetic diversity of human population and a

25   ZIKV strain from a recent clinical isolate. Through a combination of *in vitro* and *in vivo*

26   approaches, we demonstrate that multiple host genetic variants determine viral replication in

27   infected cells, and clinical severity, kinetics of blood viral load and brain pathology in mice. We

28   describe new mouse models expressing high susceptibility or resistance to ZIKV and to other

29   flaviviruses. These models will facilitate the identification and mechanistic characterization of

30   host genes that influence ZIKV pathogenesis.

31

32   **KEYWORDS**

33   Zika virus, flavivirus, mouse model, host genetics, genetic diversity, Collaborative Cross

34

35

Zika virus (ZIKV) is a mosquito-borne flavivirus isolated in 1947 from a febrile rhesus monkey in Uganda (1). Until 2007, ZIKV had circulated in Africa and Asia causing mild flu-like syndromes, with rare reported clinical cases (2). However, during recent epidemics, ZIKV infection triggered severe complications including Guillain-Barré syndrome and encephalitis in adults (3, 4), and congenital malformations in fetuses of infected pregnant women (5, 6). Viral mutations may have contributed to ZIKV enhanced pathogenicity (7, 8) but only partly explain the variable proportions of symptomatic infections (9) and the increased incidence of congenital Zika syndrome (CZS) in Polynesia (10) and Brazil (11), suggesting a role for host genetic variants. Recent evidence indicates that the regulation of innate immunity genes is driven by host genetic background in human fetal brain-derived neural stem cells (hNSCs) infected *in vitro* with ZIKV (12). Additionally, the analysis of pairs of dizygotic twins exposed to ZIKV during pregnancy and discordant for CZS suggests multigenic host susceptibility to ZIKV-induced brain malformations (13).

Multiple mouse models have been proposed to decipher the mechanisms of ZIKV disease pathogenesis (14, 15). These models allow the investigation of several key features of human infection, such as neuronal damage (16, 17), sexual and vertical transmission (18-21), fetal demise and CZS (22-25). However, while non-structural ZIKV proteins efficiently inhibit innate antiviral responses in humans (26, 27) allowing viral replication, ZIKV replicates poorly in wild-type mice due to its NS5 protein's inability to antagonize STAT2 and type I interferon (IFN) response as in humans (28). Effective systemic infection in mice occurs when this response is abrogated by genetic inactivation of the *Ifnar1* gene (29) or by blocking the type I IFN receptor with the MAR1-5A3 monoclonal antibody (mAb) (30, 31). So far, host genetic factors involved in mouse susceptibility to ZIKV infection have been investigated mainly through reverse genetic approaches, by studying the consequences of genetic ablation of specific genes, such as innate or

4

60 adaptive immunity genes (29, 32-35). While these models have contributed to our understanding

61 of the mechanisms of ZIKV disease, they do not model the simultaneous contribution of variants

62 in multiple pathways, as would most likely be observed in the natural population. A recent study

63 has reported strain-specific differences in the susceptibility to neonatal ZIKV infection across

64 four mouse laboratory strains, affecting neuropathology and behavior in adulthood (36). More

65 extensive studies investigating the role of genome-wide genetic variations on the susceptibility to

66 ZIKV infection are needed, using mouse models that accurately reflect the phenotypic and

67 genetic diversity of the human population (37).

68   In this study, we addressed this question using the two types of susceptible mouse

69 models. First, since the phenotype of a single gene modification often varies under the influence

70 of modifier genes (38, 39), we assessed the effect of host genetic background on the

71 susceptibility of *Ifnar1*-deficient mice. We then investigated the impact of host genetic diversity

72 on the susceptibility to ZIKV infection in the Collaborative Cross (CC), a panel of recombinant

73 inbred mice produced by a systematic cross between eight founder inbred strains, including five

74 classic laboratory strains and three wild-derived strains (40). The founder strains capture

75 approximately 90% of the genetic variants present in the *Mus musculus* species (41) and the

76 resulting CC strains, which segregate an estimated 45 million polymorphisms, have more genetic

77 diversity than the human population (42). Extensive variations in pathogenic phenotypes have

78 been previously reported in the CC panel after viral (43-50), bacterial (51, 52) and fungal (53)

79 infections, demonstrating that this resource is ideally suited for investigating the role of host

80 genetic variants in the pathophysiology of infectious diseases (54).

81   Susceptibility to ZIKV in *Ifnar1*-deficient mice was strongly influenced by the genetic

82 background, with practical implications for virology studies and allowing for future

83   identification of modifier genes. The challenge of 35 immunocompetent CC strains with ZIKV

84   after MAR1-5A3 mAb treatment allowed efficient viral replication. We show that genetic

85   diversity in the CC panel enabled large variations in the clinical severity of ZIKV disease, in the

86   peak and kinetics of plasma viral load and in the severity of ZIKV-induced brain pathology.

87   Genetic diversity also resulted in differences in the permissiveness of CC mouse cells to viral

88   replication which likely contributes to the *in vivo* phenotypic range. In a subset of CC strains, we

89   found correlated differences of susceptibility to ZIKV, dengue virus (DENV) and West Nile

90   virus (WNV), suggesting shared underlying mechanisms. We identified highly susceptible and

91   resistant mouse strains as new models to investigate the mechanisms of human ZIKV disease and

92   other flavivirus infections. Finally, genetic analysis revealed that susceptibility to ZIKV in the

93   CC is driven by multiple loci with small individual effects, and that *Oas1b*, a major determinant

94   of mouse susceptibility to WNV, is not involved.

95

RESULTS

Genetic background controls the susceptibility of *Ifnar1*-deficient mice to ZIKV

Many studies have used *Ifnar1* knock-out mice on 129S2/SvPas (129) (55, 56) or C57BL/6J (B6) (23, 29, 34) inbred backgrounds, but the differences in ZIKV susceptibility between these two strains have not been reported and remain unclear due to heterogeneous experimental conditions between studies. We compared the susceptibility of age-matched 129S2/SvPas-*Ifnar1*$^{-/-}$ (129-*Ifnar1*) and C57BL/6J-*Ifnar1*$^{-/-}$ (B6-*Ifnar1*) mice infected intraperitoneally (IP) with 10^7 FFUs of FG15 ZIKV. B6-*Ifnar1* mice showed increasingly severe symptoms, with body weight loss, ruffled fur, ataxia and hind limb paralysis from day 4 p.i. and were all (10/10) moribund or dead by day 7 p.i.. By contrast, 129-*Ifnar1* mice developed mild symptoms (ruffled fur, hunched back) from day 6 p.i. with only one mouse dying on day 9 p.i. while the others recovered (FIG 1), demonstrating that the susceptibility to ZIKV infection conferred by *Ifnar1* genetic inactivation is critically influenced by the host genetic background.

mAb blockade of IFNAR is a robust model to study ZIKV infection in CC mice

Ifnar1 genetic deficiency abrogates permanently IFN-α/β-mediated immune responses but is not currently available on diverse genetic backgrounds. We therefore tested the suitability of transient IFNAR blockade mediated by mAb treatment as a model to study ZIKV infection in genetically diverse mice like the CC. Since MAR1-5A3 mAb was generated in a laboratory strain (129-*Ifnar1* mice) (30), we first assessed its efficacy by Western Blot analysis on mouse embryonic fibroblasts (MEFs) isolated from two CC strains (CC001 and CC071) both of which inherited the *Ifnar1* allele from the CAST/Ei wild-derived strain (57), by comparison with B6 MEFs. IFNAR stimulation by IFN-α/β activates the JAK1/TYK2 pathway and results in the phosphorylation of STAT1. We found that, in B6, CC001 and CC071 MEFs, STAT1

119   phosphorylation was equally induced by murine IFN-α and fully inhibited by the MAR1-5A3

120   mAb (FIG 2A).

121   To assess MAR1-5A3 mAb efficacy *in vivo*, we infected CC001 and CC071 strains with 10^7

122   FFUs of FG15 ZIKV IP and we measured the kinetics of plasma viral load in mice with and

123   without 2 mg mAb treatment 24 hours prior to infection. Consistent with previous studies in B6

124   (29, Smith, 2017 #31, Scott, 2018 #25) and BALB/c (58) mice, viral load was consistently 4 to 5

125    $\log_{10}$ units higher in mAb-treated mice of both CC001 and CC071 strains compared to untreated

126   mice, demonstrating that MAR1-5A3 mAb treatment successfully increases CC mice

127   permissiveness to ZIKV replication (FIG 2B).

128   We then measured the kinetics of plasma viral load in 129-*Ifnar1* strain as well as in four

129   mAb-treated CC strains infected with 10^7 FFUs of FG15 ZIKV IP. We established that the peak

130   plasma viral load occurred in most individuals at day 2 p.i., independently of mouse genetic

131   background (FIG 2C).

132   In previous studies, viral loads have been measured either by FFU titration or by RT-qPCR

133   quantification of viral genome copies. We compared these two methods in B6-*Ifnar1*, 129-

134   *Ifnar1*, and in ten mAb-treated CC strains. We performed Focus Forming Assays (FFA) to

135   measure viral particles in the plasma at day 2 p.i. and confirmed the production of infectious

136   ZIKV in the blood of all strains (FIG 2D). Next, we compared the plasma viral load measured by

137   RT-qPCR and by FFA. We found that these two parameters were strongly correlated over a 2

138    $\log_{10}$ range (Pearson coefficient, $r^2=0.89$, $p=9.9 \times 10^{-17}$), with the number of genome copies being

139   on average 3 $\log_{10}$ units higher than the number of FFUs (FIG 2D). We therefore validated that

140   RT-qPCR measurement of plasma viral load could be used as a labor-efficient proxy for viremia

141   throughout the study.

8

142   Finally, we compared plasma viral load at day 2 p.i. between males and females in 129-

143   *Ifnar1* and in four mAb-treated CC strains in which both sexes had been tested. We found no

144   significant difference between sexes across diverse genetic backgrounds (two-way ANOVA,

145   p=0.24; FIG 2E), validating the use of merged data from males and females in mouse ZIKV

146   infection experiments.

CC genetic diversity drives ZIKV disease severity and plasma viral load

148   To explore broad genetic variation, we assessed the susceptibility of mAb-treated mice of 35

149   CC strains. B6-*Ifnar1*, 129-*Ifnar1* and mAb-treated B6 mice were included as reference strains.

150   Only mice from three CC strains developed symptoms as shown on FIG 3A which summarizes

151   clinical observations at day 7 p.i. CC021 and CC026 mice recovered and survived, while

152   symptoms worsened in 7/9 (78%) CC071 mice which were moribund or died between days 7 and

153   9 p.i.

154   Plasma viral load was measured on days 2 and 6 p.i. At day 2 p.i., which corresponds to its

155   peak, viral load was generally characterized by small within-strain heterogeneity and large inter-

156   strain variations spread over a 2.8 log_{10} range (FIG 3B), demonstrating a strong effect of host

157   genes (Kruskal-Wallis, p=$4.8x10^{-15}$) with a broad sense heritability of 86% (59). The three

158   symptomatic CC strains showed the highest peak viral load, close to that of B6-*Ifnar1* and 129-

159   *Ifnar1* mice. However, other strains (such as CC005 and CC061) had similarly high viral loads

160   but never showed any clinical signs of disease, indicating that peak viral load is unlikely the sole

161   factor controlling clinical severity. At day 6 p.i., within-strain variations were larger and more

162   heterogeneous, but we still observed highly significant inter-strain differences (Kruskal-Wallis,

163   p=$1.1x10^{-10}$). Interestingly, viral load on days 2 and 6 p.i. were only moderately correlated

164   (Pearson coefficient, r²=0.46; p=0.004), indicating that viral load at day 2 p.i. was not predictive

165   of viral load at day 6 p.i. (see for example CC018 and CC040, or CC026 and CC071).

9

166   We used the difference of the $\log_{10}$ plasma viral loads between days 2 and 6 p.i. to estimate

167   the clearance rate of the virus from the blood stream (FIG 3C; strains sorted by increasing

168   clearance rate, therefore differently from FIG 3A and B). This rate varied over a 3.3 $\log_{10}$ range

169   between strains, demonstrating a strong effect of host genes (Kruskal-Wallis, p=2.2x10^{-12}) with a

170   broad sense heritability of 76%. Likewise, B6-*Ifnar1* mice showed a slower decrease in viral

171   load than 129-*Ifnar1* mice (Wilcoxon, p=1.7x10^{-5}), despite similar peak viral load at day 2 p.i.

172   Overall, genetic diversity in the CC panel controlled clinical severity of ZIKV infection,

173   mouse survival, and the peak and clearance rate of plasma viral load. Of note, there was no

174   association, across the 35 CC strains tested, between the peak plasma viral load and the *Ifnar1*

175   allele inherited from the founder strain (ANOVA, p>0.09). This analysis confirms our *in vitro*

176   data (FIG 2A) and indicates that the variations in peak plasma viral load do not result from

177   differences in mAb treatment efficacy due to the *Ifnar1* alleles.

178   From this screening, we identified several strains with extreme phenotypes, in particular

179   CC071 which was the most susceptible to ZIKV infection, CC001, CC011, CC017 or CC060

180   with low peak plasma viral load, CC040 with slowly decreasing plasma viral load and CC045 or

181   CC026 with high peak but fast-decreasing plasma viral loads.

182   **CC mice show correlated susceptibility to ZIKV, DENV and WNV**

183   We further characterized three CC strains (indicated by arrows on FIG 3B and FIG 3C)

184   among those showing lowest (CC001) and highest peak viral loads with (CC071) or without

185   (CC005) clinical symptoms. To establish whether the above differences were specific of the

186   FG15 ZIKV strain of the Asian lineage, we first assessed the susceptibility of the three selected

187   strains to the HD78788 ZIKV strain of the African lineage. 129-*Ifnar1* mice and mAb-treated

188   CC mice were infected with 10^3 FFUs of HD78788 ZIKV IP which proved to be highly

189   pathogenic in *Ifnar1*-deficient mice with rapid and severe symptoms and 100% mortality (FIG

190   4A). CC001 was fully resistant with no or mild clinical signs (FIG 4A, left and center panels).

191   By contrast, all CC071 mice were moribund or dead by day 10 p.i., with early and quickly

192   aggravating symptoms, almost like 129-*Ifnar1* mice. Only 1/5 CC005 mouse died with late

193   symptoms. Peak viral load (day 2 p.i.) varied over a 2.4 $\log_{10}$ range and the differences between

194   strains were similar to those observed with the FG15 ZIKV strain (FIG 3B). Here again, plasma

195   viral load at day 2 p.i. was the highest in very susceptible CC071 and 129-*Ifnar1* strains and low

196   in resistant CC001, but it was also very high in CC005 which was moderately susceptible,

197   confirming that clinical severity does not depend solely on peak plasma viral load.

198   To evaluate whether these differences in susceptibility were specific to ZIKV or extended to

199   other flaviviruses, we assessed the phenotype of a few strains after infection with DENV and

200   WNV, two other members of the *Flaviridae* family.

201   We measured plasma viral load after IV infection with $2x10^6$ FFUs of KDH0026A DENV in

202   mAb-treated CC001, CC071 and B6 mice and in 129-*Ifnar1* and B6-*Ifnar1* mice (FIG 4B right).

203   Most inter-strain differences observed with ZIKV FG15 strain (FIG 4B left, data from FIG 3B)

204   were conserved with DENV, CC071 displaying the highest plasma viral load in Ab-treated mice.

205   DENV infection was overall much less clinically severe since only B6-*Ifnar1* mice developed

206   non-lethal symptoms including ruffled fur, hunched back and ataxia.

207   We also investigated the susceptibility of the selected CC strains to WNV. *Oas1b* was

208   previously shown to be a major host genetic determinant of susceptibility to WNV in mice (60).

209   Of note, the three selected CC strains carry the same non-functional allele of *Oas1b* inherited

210   from the laboratory strain founders, conferring them susceptibility to WNV infection. CC mice

211   were infected IP with 10^4 FFUs of WNV IS-98-ST1 and monitored for 14 days p.i. (WNV

212   infection does not require anti-IFNAR mAb treatment in *Oas1b*-deficient mice). All CC071 mice

213   died 7 days p.i., significantly faster than CC001 and CC005 mice (logrank, p<0.01; FIG 4C, left

214   panel), indicating that genetic diversity between CC strains also influences their susceptibility to

215   WNV even in the context of *Oas1b* deficiency.

216   To assess whether the differences of susceptibility between these CC strains also applied to

217   other viruses, we infected them with 10^2 PFUs of RVFV ZH548 IP. No significant difference

218   was found between CC strains (logrank, p>0.05 for all pair comparisons; FIG 4C, right panel)

219   which succumbed late from the infection, like the commonly used BALB/cByJ mice.

220   **Genetic analysis suggests a polygenic control of susceptibility to ZIKV in CC mice**

221   To identify host genetic factors controlling the susceptibility to ZIKV in CC strains, we

222   performed a genome-wide association study between the plasma viral loads at days 2 and 6 p.i.

223   or the decrease rate of plasma viral load, and the genotypes of the 35 CC strains. Genetic

224   associations were plotted as LOD scores (FIG 5). We did no find genome locations at which

225   LOD scores reached the minimum 0.1 significance threshold for any of the three traits, while it

226   would be expected if phenotypic variations were controlled by one or two loci with strong

227   effects. Therefore, these results suggest that plasma viral load is controlled by multiple small-

228   effect genetic variants.

229   **Genetic diversity of CC strains controls brain viral load and pathology**

230   To assess the influence of host genetics on the brain pathology caused by ZIKV infection,

231   we further characterized the three previously selected CC strains. We measured the viral load in

232   the brain 6 days after IP infection with FG15 ZIKV in mAb-treated CC mice and 129-*Ifnar1*

233   mice (FIG 6, top). CC005 and CC071 which had higher peak plasma viral load also had higher

234   brain viral load (FIG 6, mean=6.5 $\log_{10}$ copies/µg RNA for CC005 and CC071, compared with 5

235    $\log_{10}$ copies/µg RNA for CC001). As expected, 129-*Ifnar1* mice showed the highest viral load in

236   the brain. These results indicate overall correlation between plasma and brain viral loads.

237   Histopathological analysis, carried out in the brain of the same mice (FIG 6 bottom),

238   revealed different lesion profiles between the four mouse strains. 129-*Ifnar1* mice indeed

239   displayed the most severe inflammatory lesions (subacute leptomeningo-encephalitis). By

240   contrast, almost no lesions were detected in the brain of CC001 mice. CC005, and CC071

241   displayed only minimal to mild encephalitis (more severe for CC005 mice), but with activation

242   of microglial cells and microglial nodules similar to that of 129-*Ifnar1* mice, as revealed by Iba1

243   immunolabeling.

244   The nature and intensity of brain histological lesions may depend on the circulating viral

245   load, on the capacity of the virus and of the mAb to cross the blood-brain barrier and on the

246   permissiveness of brain cells (in particular neurons and microglia). To assess the differences in

247   susceptibility of brain cells between CC strains, we performed intra-cerebral infections to deliver

248   the virus directly into the brain tissue. 129-*Ifnar1* and mAb-untreated CC mice received 10^5

249   FFUs of FG15 ZIKV in the left ventricular region of the brain and were followed for 3 weeks.

250   Mild and transient symptoms (ruffled fur, hunched back) were observed in a few mice of the

251   three strains and one CC005 mouse died on day 19 p.i. A second group of CC mice were infected

252   similarly and euthanized at day 6 p.i. for histological analysis. Differences in brain viral load

253   between CC strains were similar to those observed after IP infection, with CC005 and CC071

254   mice showing significantly higher brain viral load than CC001 mice (FIG 7, top). Compared with

255   IP route of infection, lesions in 129-*Ifnar1* mice were mostly similar, while lesion profiles were

256   clearly different in the three CC strains (FIG 7, bottom). Strikingly, the most severe lesions were

257   detected for CC071, with marked subacute leptomeningo-encephalitis and strong activation of

258   microglial cells (Iba1 staining). CC001 and CC005 mice also displayed inflammatory lesions,

259   clearly less severe than CC071, with gliosis, microglia activation and microglial nodules.

13

260   These results indicate that CC strains differ in their permissiveness to viral replication in the

261   brain and in their susceptibility to ZIKV-induced histological brain damage, independently from

262   potential differences in the capacity of ZIKV to disseminate to the brain from the circulation.

263   **Viral replication in CC071 cells is increased *in vitro***

264   Differences in peak plasma viral load and results from IC infections suggested that different

265   rates of viral replication could contribute to the variations in susceptibility between CC strains.

266   To address this point, we measured the production of viral particles in three cell types infected

267   with ZIKV FG15. We derived primary MEFs, peritoneal macrophages (PMs) and primary

268   cultured neurons (PCNs) from CC001 and CC071 strains. Cells were infected with ZIKV FG15

269   at a MOI of 5. In all three cell types, CC071 cells produced increasingly higher amounts of viral

270   infectious particles than CC001 cells between 24 and 72 hours (FIG 8). These results suggest that

271   increased replication rate in CC071 could contribute to its susceptible phenotype.

272

14

273 **DISCUSSION**

274   ZIKV is a serious public health concern considering the occurrence of severe neurological

275 complications in adults and congenital malformations that can result from the infection of

276 pregnant women. The variable outcomes of ZIKV infection in humans has led to hypothesize a

277 role for host genetic factors (9, 13) although this has never been demonstrated thus far. As for

278 other infectious diseases, human genetic studies on susceptibility to ZIKV would require large

279 cohorts of patients and would be confounded by pathogen genetics, pathogen dose, mosquito-

280 dependent factors and multiple environmental parameters.

281   Several mouse models of human ZIKV infection have already been described and have

282 substantially improved our understanding of viral tropism, dissemination, pathogenesis,

283 persistence, transmission and vaccine protection. To overcome the inability of ZIKV to inhibit in

284 mice IFN induction and signaling pathways as observed in humans (27), most studies have been

285 performed using *Ifnar1*-deficient mice which have become a reference model. However, high

286 levels of viral replication can also be achieved by temporary inhibition of IFN signaling by anti-

287 IFNAR mAb treatment (30, 31, 61) or even in immunocompetent mice by infecting neonates

288 (36, 62-64) or using a combination of mouse-adapted ZIKV strains and human STAT2 knock-in

289 mice (65).

290   The choice of the ZIKV strain used in an animal model is important to maximize the

291 relevance of mouse studies to human infection. Mouse studies have used different ZIKV strains

292 from the African or Asian lineages. Mouse-adapted strains of the African lineage derived from a

293 large number of serial passages are more pathogenic in mice at lower doses (34) but carry

294 mutations that may bias the translatability of results to humans. To avoid this limitation, mouse

295 studies have often used different ZIKV strains from the Asian lineage derived from clinical

296 isolates. Genetic differences between these two lineages are suspected to be responsible for the

15

297   emergence of symptomatic cases in human starting with the Yap Island epidemics in 2007 (7, 8).

298   Therefore, while the ZIKV strain needs to be standardized in experimental studies, generalization

299   of the results obtained with one viral strain require confirmation using another strain. Because of

300   the incidence of neurological complications associated with infections by Asian lineage ZIKV,

301   we used for our genetic screening a low-passage strain derived from a 2015 case of French

302   Guyana, at an early stage of the South-American epidemics. Since this strain had not been

303   adapted to the mouse, high doses were required to achieve high circulating viral loads.

304   Most mouse studies have used either B6-*Ifnar1* or 129-*Ifnar1* strains without specific

305   rationale and their results cannot be directly compared due to many experimental differences

306   such as ZIKV strain, dose and route of inoculation (66). Under strictly identical conditions, we

307   found that B6-*Ifnar1* mice developed more rapid and severe clinical symptoms and higher

308   mortality than 129-*Ifnar1* mice, despite similar levels of plasma viral RNA at day 2 p.i. We also

309   found that viral load persisted longer in B6-*Ifnar1* mice. These results show that, under our

310   experimental conditions, these two *Ifnar1*-deficient strains have clearly distinct susceptibility to

311   ZIKV. To our knowledge, these two strains have been compared in only one study which found

312   no difference in survival after WNV infection (67). However, their extreme susceptibility might

313   have prevented the identification of any difference. Our results have practical implications for

314   many studies based on *Ifnar1*-deficient mice and motivate further genetic studies to identify the

315   determinants and mechanisms controlling differences of susceptibility between B6 and 129

316   inbred backgrounds.

317   To further investigate the role of host natural genetic variants on ZIKV susceptibility, we

318   leveraged the genetic diversity across CC strains. The CC has been developed as a collection of

319   inbred strains that more accurately reproduce the genetic diversity and phenotypic range seen in

320   human population (68). To enable systemic ZIKV replication after parenteral inoculation in

16

321 diverse genetic backgrounds, we blocked type I IFN response using MAR1-5A3 mAb (23, 31).

322 However, because CC genetic diversity includes sequence polymorphisms in the *Ifnar1* gene

323 which could affect the efficacy of mAb-mediated IFNAR inhibition, we confirmed full

324 abrogation of IFNα-induced STAT1 phosphorylation in MEFs from two CC strains carrying a

325 wild-derived *Ifnar1* haplotype. Moreover, we showed that the differences in peak plasma viral

326 load across 35 CC strains were not associated with the *Ifnar1* allele each CC has received from

327 the founder strains. These results validate that the MAR1-5A3 mAb has similar efficacy across a

328 broad range of mouse genetic backgrounds, which will be useful to develop new models of viral

329 infections.

330 A single injection of MAR1-5A3 mAb 24 hours before ZIKV infection resulted in moderate

331 to very high levels of viral RNA in the blood and brain. ZIKV infection was symptomatic in a

332 minority of CC strains (3/35), as observed in infected humans (9, 69), and mortality was

333 observed only in CC071. These results confirm that ZIKV can replicate and establish viremia

334 without inducing symptoms (29). Moreover, while all symptomatic strains had high peak viral

335 loads, other strains with similar viral loads (like CC005 or CC061) never developed any signs of

336 illness, indicating that other pathogenic mechanisms are required to result in symptomatic

337 infection and that viral load alone does not reliably predict clinical outcome of ZIKV infection in

338 a genetically diverse mouse population.

339 Since all experimental parameters were carefully standardized between strains (in particular,

340 the microbiological environment in which they were bred), which resulted in small intra-strain

341 variations, and since the MAR1-5A3 mAb treatment was similarly effective across strains,

342 differences in peak viral load between strains can be confidently attributed to host genetic

343   variants. The 86% broad sense heritability further indicates that genetic background is the

344   principal factor driving peak viral load across CC strains.

345   Viremia decreased between days 2 and 6 p.i., as previously reported in several studies (55,

346   70, 71) but not in others (29, 56) for reasons that have not been discussed and remain unclear. In

347   our study, the rate of decrease, which was estimated as the difference in viral load between day 2

348   and day 6 p.i., showed remarkable homogeneity between individuals of the same CC strain and

349   very large variations across CC strains. This data resulted again in high broad sense heritability

350   which demonstrates a strong influence of host genes on this trait. The decrease of circulating

351   viral load is the net result of ZIKV production in infected tissues, dissemination to the blood

352   stream and elimination from the circulation. Therefore, host genes could control the kinetics of

353   viral load through multiple mechanisms.

354   After exploring the range of susceptibility to ZIKV across broad genetic diversity, we

355   focused our study on a few CC strains exhibiting contrasted phenotypes with the aim of

356   characterizing new models (72). CC001 is one of the least permissive to ZIKV, with low peak

357   viral load. At the other extreme of the distribution, CC005 and CC071 have similarly high

358   plasma viral loads while only CC071 shows symptoms and high mortality. These differences

359   between CC strains were strikingly conserved with the African, mouse-adapted, HD78788 strain

360   (FIG 4A). The use of lower infectious doses with HD78788 virus was supported by its higher

361   pathogenicity resulting from mouse adaptation. The consistency between these two experiments

362   suggest that the large phenotypic diversity we have reported should apply to most ZIKV strains.

363   Overall, brain viral load and brain pathology after IP infection were consistent with peak

364   plasma viral load. In CC mice, the most notable microscopic lesions included signs of

365   neuroinflammation evidenced by Iba1 immunohistochemistry. Neuroinflammation was similar in

366   129-*Ifnar1*, CC005 and CC071 mice. These changes were less pronounced than in a previous

367 study which reported more severe CNS lesions in MAR1-5A3-treated B6 mice (31), infected

368 with a more virulent African lineage ZIKV strain. The variable severity of lesions observed in

369 CC mice, ranging from very mild abnormalities in CC001, to inflammatory lesions with

370 perivascular cuffing, activation of microglial cells and microglial nodules in CC005, indicates

371 that the genetic background also controls ZIKV neuropathogenesis.

372 The less severe histological lesions observed in CC mice compared with 129-*Ifnar1* mice

373 could be due to the limited access to the brain of the virus or of the mAb which does not

374 appreciably cross the blood-brain barrier (29). Therefore, intracerebral infection aimed at

375 comparing brain lesions between strains while controlling the amount of virus effectively

376 delivered. Surprisingly, CC001 and CC005 mice showed similar types and severity of lesions

377 (although not all CC001 mice showed lesions) while CC071 mice developed much more severe

378 signs of leptomeningo-encephalitis with massive neuroinflammation, similar to those of 129-

379 *Ifnar1* mice. This last result suggests that the milder lesions observed in CC071 compared with

380 129-*Ifnar1* mice after IP infection were likely due to reduced viral dissemination to the brain.

381 Importantly, mice did not receive prior mAb treatment, allowing for the development of local

382 and systemic antiviral responses. These results emphasize the complex interplay between

383 infected cells and effectors of the immune response, which likely differs between CC strains

384 under the control of host genes.

385 Viral replication rate between resistant CC001 and highly susceptible CC071 mice was

386 investigated as a plausible mechanism for the differences in susceptibility between these two

387 strains. MEFs are a semi-permanent source of cells which have been extensively used to assess

388 viral replication (73, 74) including with ZIKV (75, 76). Although not the primary target of ZIKV

389 infection, macrophages are also a relevant cell type to investigate ZIKV replication and innate

390 responses (77). Mouse peritoneal macrophages are more easily recovered than MEFs (78)

391 although they can only be used as a primary culture. Finally, primary cultured neurons are of

392 particular relevance considering ZIKV tropism for neural progenitors (63). Although the kinetics

393 of viral replication were different between cell types, with a swift drop in CC001 macrophages at

394 48h while it was slower in CC001 MEFs and primary neurons, replication steadily increased

395 over time in all three cell types of CC071 origin, leading to significantly higher viral titers at

396 72h. Our data is consistent with the observation by Caires-Junior et al. who reported increased

397 ZIKV replication rate in iPS-derived neuroprogenitor cells from CZS-affected babies compared

398 with their unaffected dizygotic twin (13). Therefore, our results strongly suggest that increased

399 replication rate in CC071 compared with CC001 likely contributes to its higher plasma and brain

400 viral loads and to its higher overall susceptibility to ZIKV.

401   Investigating the genetic diversity of a large number of CC strains has significantly extended

402 the range of phenotypes induced by ZIKV infection in mice and better model the heterogeneity

403 of the human population. It has allowed testing important factors such as mouse gender and the

404 method of viral load measurement across multiple host genetic background, providing robust

405 conclusions (37). Importantly, we found no differences between male and female mice in their

406 susceptibility to ZIKV disease, nor in the peak viral load (FIG 2E). We also found a high

407 correlation between viral loads measured by titration and by qRT-PCR over a 2 $\log_{10}$ range (FIG

408 2D). This is in contrast with a study on Ebola virus which showed that, in spleen and liver, the

409 susceptible mice produced similar amounts of viral genomes but 1 to 2 $\log_{10}$ more infectious

410 virions than the resistant mice (43).

411   Genetic diversity also allowed us to assess correlations between traits, which cannot be

412 achieved in a single strain. We showed that brain viral load was consistent with plasma viral

413 load, but that plasma viral loads at days 2 and 6 p.i. were only moderately correlated. Likewise,

414 we found that clinical severity did not correlate with the intensity of brain histological lesions

20

415   and neuroinflammation, as summarized in Table 1. These dissociations between phenotypes

416   provide evidence for partly distinct mechanisms and genetic control (37) and result in distinct

417   mouse models.

418   A recent study has reported strain-dependent variations in the long-term neuropathological

419   and behavioral consequences of ZIKV infection after neonatal infection between four mouse

420   inbred strains known to differ in their susceptibility to pathogens (36). Since they are all

421   laboratory strains, they do not cover the same genetic variation as in our study and it is likely that

422   even more diverse phenotypes would be observed in this model with the CC panel.

423   Genetic analysis of our results strongly suggests that, by contrast with other viruses for

424   which major host genetic determinants have been identified (e.g. *Oas1b* for WNV (60) or *Mx1*

425   for influenza virus (79)), susceptibility to ZIKV in CC strains is under polygenic control. This is

426   supported by the continuous distributions of peak plasma viral load (FIG 3B) and of the rate of

427   viral decrease (FIG 3C), and by the absence of any regions of the genome significantly

428   associated with variations in viral load (FIG 5). Calculations based on CC genotypes show that,

429   with 35 strains and an average of 5 mice per strain, we had 80% power of detecting a bi-allelic

430   QTL explaining 30% or more of the phenotypic variance (80). This clearly rules out the

431   possibility that the phenotypic variations measured across CC strains were controlled by one or

432   few genes with major effects, as observed with *Oas1b* for WNV (47). Dissecting the genetic

433   architecture of resistance and susceptibility to ZIKV in these strains will require dedicated

434   intercrosses (72).

435   *Oas1b* is an interferon-stimulated gene and a major determinant of mouse susceptibility to

436   WNV (45). A variant in OAS3, a member of the human homologous gene family, has been

437   associated with increased severity of dengue (81). Most laboratory strains, including five of the

438   eight CC founders, carry the same non-functional allele of *Oas1b* which renders them susceptible

21

439   to WNV infection (60), while the three wild-derived CC founders carry polymorphic but

440   functional alleles and are resistant (45). CC strains therefore carry either functional or non-

441   functional *Oas1b* alleles. Our results provide multiple lines of evidence to rule out a significant

442   role of *Oas1b* in the variations of susceptibility to ZIKV across CC strains. First, since mAb-

443   mediated blockade of type I IFN response likely inhibits temporarily *Oas1b* induction, *Oas1b*

444   allele is unlikely to explain differences in peak viral load at day 2 p.i. Moreover, our QTL

445   mapping analysis showed that mouse genotype at *Oas1b* (located on distal chromosome 5) did

446   not significantly contribute to variations in viral load at day 2 or day 6 p.i., or in the rate of viral

447   load decrease (FIG 5). Finally, since both CC001, CC005 and CC071 strains carry the *Oas1b*

448   deficient allele (http://csbio.unc.edu/CCstatus/CCGenomes/), their differences in clinical

449   severity, brain pathology and replication rate in infected cells must be controlled by other genetic

450   variants. Interestingly, the large difference of survival time after WNV infection between CC071

451   and CC001 or CC005 provides ideal strain combinations to identify novel genes controlling

452   susceptibility to this virus.

453   Out of this large series of CC strains, we identified several new mouse models of ZIKV

454   disease. CC071 mice were the most susceptible to ZIKV infection, more than mAb-treated B6

455   mice (FIG 3A,B). mAb treatment was required to achieve high circulating viral load (FIG 2B),

456   showing that CC071 has functional type I IFN response. CC071 mice were also very susceptible

457   to DENV and WNV, two flaviviruses related to ZIKV. However, they are not uniformly

458   susceptible to infectious agents since they showed susceptibility to RVFV similar to that of

459   BALB/c, CC001 and CC005 mice, and intermediate susceptibility to *Salmonella* Typhimurium

460   (52). Together with other susceptible strains like CC021 and CC026 which developed symptoms,

461   or CC005 which developed severe brain lesions, CC071 will help identifying mechanisms of

462   severe ZIKV infection and their genetic control. By contrast, CC001 mice were highly resistant,

463   even to a strongly pathogenic African ZIKV strain, despite blockade of type I IFN signaling.

464   Extensive analysis of these CC strains with extreme phenotypes may elucidate how genetic

465   variants affect susceptibility as well as innate and adaptive immune responses to flaviviral

466   infection (72) and provide deeper understanding of the pathophysiology of severe complications

467   of human ZIKV disease.

468

23

469 **MATERIALS AND METHODS**

470

471 **Mice**

472   All Collaborative Cross (CC) mice (purchased from the Systems Genetics Core Facility,

473 University of North Carolina and bred at the Institut Pasteur) (82), C57BL/6J mice (purchased

474 from Charles River Laboratories France), BALB/cByJ and *Ifnar1* knock-out mice (*Ifnar1^{tm1Agt}*

475 allele on 129S2/SvPas or C57BL/6J background, designated 129-*Ifnar1* and B6-*Ifnar1*,

476 respectively, and bred at the Institut Pasteur) were maintained under SPF conditions with 14:10

477 light-dark cycle and *ad libitum* food and water in the Institut Pasteur animal facility. In all

478 experiments, mice were killed by cervical dislocation. All experimental protocols were approved

479 by the Institut Pasteur Ethics Committee (projects #2013-0071, #2014-0070, #2016-0013, #2016-

480 0018 and dap190107) and authorized by the French Ministry of Research (decisions #00762.02,

481 #7822, #6463, #6466 and #19469, respectively), in compliance with French and European

482 regulations.

483

484 **Cell lines**

485   Vero cells (ATCC CRL-1586) were cultured at 37°C in Dulbecco's Modified Eagle Medium

486 (DMEM, Gibco) supplemented with 10% fetal bovine serum (FBS, Eurobio). C6/36 cells (ATCC

487 CRL-1660) were cultured at 28°C in Leibovitz Medium (L-15 Medium, Gibco) supplemented with

488 10% FBS, 1% Non-Essential Amino Acids (Life Technologies) and 1% Tryptose Phosphate Broth

489 (Life Technologies).

490

Viruses

The FG15 Asian Zika virus (ZIKV) strain, isolated from a patient during ZIKV outbreak in French Guiana in December 2015, was obtained from the Virology Laboratory of the Institut Pasteur of French Guiana. The HD78788 African ZIKV strain, isolated from a human case in Senegal in 1991, was obtained from the Institut Pasteur collection. The KDH0026A DENV serotype 1 (DENV-1) strain, isolated from a patient in Thailand in 2010, was previously described (83). Viral stocks were prepared from supernatant of infected C6/36 cells, clarified by centrifugation at 800g and titrated on Vero cells by focus-forming assay (FFA). Stocks were kept at -80°C. The West Nile virus (WNV) strain IS-98-ST1 (or Stork/98) was obtained, cultured and used as described in Mashimo *et al.* (60). The Rift Valley Fever virus (RVFV) strain ZH548 was obtained, cultured and used as described in Tokuda *et al.* (84).

Mouse experiments

All infection experiments were performed in a biosafety level 3 animal facility. Mice were maintained in isolators.

ZIKV and DENV systemic infection. CC mice received 2 mg of IFNAR-blocking mouse mAb (MAR1-5A3, BioXCell) by intraperitoneal (IP) injection one day before ZIKV or DENV infection (85). Groups of 6-8 week-old mice were inoculated IP with 10^7 focus-forming units (FFUs) of ZIKV FG15 or 10^3 FFUs of ZIKV HD78788, in 200µL PBS. For DENV infection, mice were anesthetized by IP injection with a solution of Xylazine (5 mg/kg) and Ketamine (80 mg/kg) and afterwards inoculated by intravenous (IV) injection in the retro-orbital sinus with 2.10^6 FFUs of DENV-1 KDH0026A, in 100µL PBS. Survival and clinical signs were monitored daily for up to 14 days. Clinical signs were scored as follows: 0, no symptom; 1, ruffled fur; 2, emaciation, hunched posture and/or hypo activity; 3, hind limb weakness, prostration and/or closed eyes; 4,

25

515   moribund or dead. Blood samples were collected at several time points from the retromandibular

516   vein for plasma viral load assessment.

517   ZIKV intracerebral infection. Mice were anesthetized by IP injection with a solution of

518   Xylazine (5 mg/kg), Ketamine (75 mg/kg) and Buprenorphine (0.03 mg/kg). Groups of 5-6 week-

519   old mice were then inoculated by intracerebral (IC) injection in the right brain hemisphere with a

520   26-gauge needle affixed to a Hamilton syringe sheathed by a wire guard allowing no more than a

521   4-mm penetrance into the skull cavity, as described in (86). Mice received either 10^5 FFUs of

522   ZIKV FG15 in PBS or PBS alone, in a volume of 10μL. Survival and clinical signs were monitored

523   daily for 6 days and euthanized for brain collection. Another cohort of mice (n=7-8 per strain) was

524   infected similarly and monitored daily for 21 days to assess symptoms and survival.

525   WNV and RVFV infection. Groups of 8-12 week-old mice were inoculated IP with 10^3 FFUs

526   of WNV strain IS-98-ST1 or 10^2 PFUs of RVFV strain ZH548. Survival and clinical signs were

527   monitored daily for up to 14 days (RVFV) or 21 days (WNV).

528

529   **Mouse embryonic fibroblasts (MEFs) isolation and infection**

530   MEFs were isolated from fetuses at day 13.5-14.5 of gestation, and cultured in DMEM

531   supplemented with 10% FBS (Eurobio) and 1% penicillin/streptomycin (Gibco) at 37°C. MEFs

532   were used until passage 2.

533   MEFs were plated at identical densities in culture dishes 24 hours before infection. MEFs

534   were infected with ZIKV FG15 strain at a MOI of 5. After 2 hours of incubation at 37°C, the

535   inoculum was replaced with fresh medium. Supernatants were collected at 24, 48 and 72 hours

536   post-infection. Titration was performed by FFA in Vero cells.

537

538   **Mouse peritoneal macrophages (PMs) isolation and infection**

26

539   Ten week-old mice were killed and PMs were collected by peritoneal lavage with 5 mL PBS

540   (Gibco). The cell suspension was filtered on a 100 µm cell strainer and centrifuged at 800g for 10

541   minutes at 4°C. The cell pellet was re-suspended in serum-free RPMI 1640 medium (Gibco) and

542   cells were plated in 96-well plates at desired density. After 1 hour incubation at 37°C, non-adherent

543   cells were removed by 2 washes with PBS and fresh RPMI 1640 medium supplemented with 10%

544   FBS and 1% penicillin/streptomycin was added to adherent cells.

545   Twenty-four hours after seeding, PMs were infected with ZIKV FG15 strain at a MOI of 5.

546   After 2 hours of incubation at 37°C, the inoculum was replaced with fresh medium. Supernatants

547   were collected at 24, 48 and 72 hours post-infection. Titration was performed by FFA in Vero

548   cells.

549

550   **Mouse primary neurons isolation and infection**

551   Primary neurons were prepared from mouse fetuses at day 16.5 of gestation. Isolated cortices

552   were rinsed in HBSS medium (Gibco) and digested with 1 mg/mL Trypsin-EDTA (Gibco) and 0.5

553   mg/mL DNase I (Merck) in HBSS medium for 15 minutes at 37°C. B-27 supplement (Life

554   Technologies) was added to inactivate Trypsin and mechanical dissociation of the cortices was

555   performed by passages through a narrowed glass pipet. The cell suspension was centrifuged for 10

556   minutes at 200g and cell pellet was re-suspended in Neurobasal medium (Gibco) supplemented

557   with 2% B-27, 0.2% L-glutamine (Gibco) and 1% penicillin-streptomycin-fungizone (Life

558   Technologies). Cells were plated at identical densities in culture plates pre-coated with polyD-

559   lysine (Merck) and Laminin (Merck).

560   Primary cultured neurons were infected with ZIKV FG15 strain at a MOI of 5 at 12 days of

561   *in vitro* culture, for network maturation. After 2 hours of incubation at 37°C, the inoculum was

562 replaced with fresh medium. Supernatants were collected at 24, 48 and 72 hours post-infection.

563 Titration was performed by FFA in Vero cells.

564

Focus-forming assay

566 Vero cells were seeded at 3.10^4 per well in 100 µl complete medium (DMEM, FBS 10%) in

567 96-well plates. After overnight incubation at 37°C, medium was replaced with 40 µL of serial 10-

568 fold dilutions of the samples, and 115 µL of methylcellulose overlay was added 2 hours later. After

569 40 hours incubation, culture medium was removed and cells were fixed with 100 µL/well of 4%

570 paraformaldehyde for 20 minutes and permeabilized with a solution of 0.3% Triton and 5% FBS

571 in PBS for 20 minutes. Cells were washed, incubated with a mouse mAb directed against ZIKV

572 envelop protein (4G2, purified from the ATCC hybridoma) for 1 hour at 37°C (1/250[e] in blocking

573 buffer). Cells were further washed, incubated with secondary antibody (AlexaFluor-488-

574 conjugated anti-mouse IgG, Invitrogen) for 45 minutes at 37°C and washed. Infected cell foci were

575 counted using an ImmunoSpot CTL analyzer and viral titers were calculated from the average

576 number of foci.

577

Viral genome quantification by RT-qPCR

579 Blood samples were centrifuged to recover plasma from which viral RNA was extracted with

580 the QIAamp Viral RNA Mini Kit (Qiagen). Brain samples were homogenized at 4°C in 1 mL of

581 TRIzol reagent (Life Technologies) using ceramic beads and automated homogenizer (PreCellys).

582 Total RNA was extracted according to manufacturer's instructions. cDNA synthesis was

583 performed using MMLV reverse transcriptase (Life Technologies) in a Bio-Rad *Mycycler*

584 thermocycler. ZIKV and DENV cDNA were quantified by TaqMan quantitative PCR (qPCR) in

585 a ViiA7 Instrument (Life Technologies) using standard cycling conditions. Primer sets adapted

586   from previous works (87-89) were used to detect ZIKV and DENV RNA. ZIKV FG15 : forward,

587   5'-CCG CTG CCC AAC ACA AG- 3'; reverse, 5'-CCA CTA ACG TTC TTT TGC AGA CAT-

588   3'; probe, 5'-6FAM-AGC CTA CCT TGA CAA GCA ATC AGA CAC TCA A-MGB- 3' (Life

589   Technologies). ZIKV HD78788: forward, 5'-AAA TAC ACA TAC CAA AAC AAA GTG GT-

590   3'; reverse, 5' -TCC ACT CCC TCT CTG GTC TTG- 3'; probe, 5'-6FAM-CTC AGA CCA GCT

591   GAA G-MGB- 3' (Life Technologies). DENV-1 KDH0026A: forward, 5' –GGA AGG AGA

592   AGG ACT CCA CA- 3'; reverse, 5'- ATC CTT GTA TCC CAT CCG GCT- 3'; probe, 5' -6FAM

593   CTC AGA GAC ATA TCA AAG ATT CCA GGG-MGB- 3' (Life Technologies). Viral load is

594   expressed on a Log_{10} scale as viral genome copies per milliliter (plasma samples) or per total RNA

595   microgram (brain samples) after comparison with a standard curve produced using serial 10-fold

596   dilutions of a plasmid containing the corresponding fragment of ZIKV genome.

597

Western Blot analysis

599   MEFs (5.10^6) were pre-incubated with IFNAR1-blocking antibody (MAR1-5A3, BioXCell)

600   for 7 hours and then stimulated, or not, with 300 IU/mL mouse IFN-α (Miltenyi Biotec) for 15

601   minutes. MEFs were detached and centrifuged at 300xg for 5 minutes and cell pellet was re-

602   suspended in cold PBS. MEFs were then lyzed into extraction buffer (10 mM Tris–HCl, pH 7.5, 5

603   mM EDTA, 150 mM NaCl, 1% NP40, 10% glycerol, 30 mM NaP, 50 mM NaFluoride) completed

604   with protease inhibitor (Complete, EDTA free, Roche) and phosphatase inhibitors (phosStop easy

605   pack, Roche) with 2.5 UI of benzonase nuclease (Sigma). Lysates were incubated on ice for 30

606   minutes and non-soluble fraction was separated by centrifugation. Protein concentrations were

607   determined by Bradford assay, and equal amounts of protein were further used. Protein

608   denaturation was performed in Laemmli buffer at 95°C for 5 minutes. After separation on a 12%

609   polyacrylamide gel (Biorad), proteins were transferred on Immun-Blot polyvinylidene difluoride

610 (PVDF) membrane (Biorad) and incubated overnight with the following antibodies: Anti-

611 Phospho-Stat1 Tyr701 (1/1,000^e, #9167, Cell Signaling), Anti-Total Stat1 N-terminus (1/500^e, #

612 610115, BD Biosciences), Anti-αTubulin (1/8,000^e, # T5168, Merck). Membranes were incubated

613 for 1.5 hour at room temperature with an anti-mouse or an anti-rabbit IgG horseradish peroxidase-

614 linked secondary antibody (1/10,000^e, NA931 and NA934V, Amersham) and signals were

615 visualized using autoradiography.

616

617 **Histopathology**

618 After necropsy, brain was removed, fixed for 48-72 hours in 10% neutral-buffered formalin

619 and embedded in paraffin; 4µm-thick sections were stained in hematoxylin-eosin. Morphology of

620 microglial cells was assessed by immunohistochemistry using rabbit anti-Iba1 primary antibody

621 (# 01919741, Wako chemical, dilution 1:50) as previously described (90). Sections were analyzed

622 by a trained veterinary pathologist in a blind study on coded slides.

623

624 **Genetic analysis**

625 Broad sense heritability was calculated as previously described (59).

626 Plasma viral load at days 2 and 6 p.i. and plasma viral load decrease, measured on 159 mice

627 from 35 CC strains (average of 4.5 mice per strain), were used in quantitative trait locus (QTL)

628 mapping using the rqtl2 R package (91) and GigaMUGA genotypes of CC founders and CC strains

629 available from http://csbio.unc.edu/CCstatus/CCGenomes/#genotypes. Genome scan was

630 performed using the scan1 function with a linear mixed model using a kinship matrix. Statistical

631 significance levels were calculated from 1,000 permutations.

632 Genotype-phenotype associations for specific genes (*Ifnar1*, *Oas1b*) were tested by Kruskal-

633 Wallis test using the founder haplotype as the genotype.

30

634

Statistical analysis

636 Statistical analyses were performed using R software (v3.5.2). Kaplan-Meier survival curves

637 were compared by logrank test. Two-way ANOVA was used for testing mouse strain and sex

638 effects on plasma viral load at day 2 p.i. (FIG 2E). Student's *t*-test was used to compare viral loads

639 in tissues, except when data showed heterogeneous variance between groups, in which case we

640 used Kruskal-Wallis and Wilcoxon non-parametric tests. These tests were also used for assessing

641 mouse strain effect on plasma viral load and on plasma viral load decrease (FIG 3). Pearson's

642 coefficient was used for the correlation between plasma viral load at days 2 and 6 p.i. (FIG 3B)

643 and for the correlation between measurements of plasma viral load by FFA and RT-qPCR (FIG

644 2D). Student's *t*-test was used to compare viral titers between strains in *in vitro* experiments. P-

645 values < 0.05 were considered statistically significant.

646

647

NOTES

31

658   The authors declare no competing interests.

659   This work was supported by a grant from the French Government's Investissement d'Avenir

660   program, Laboratoire d'Excellence "Integrative Biology of Emerging Infectious Diseases" (grant

661   n°ANR-10-LABX-62-IBEID). C.M. was supported by a fellowship from the grant n°ANR-10-

662   LABX-62-IBEID.

663

REFERENCES

1. **Petersen LR, Jamieson DJ, Powers AM, Honein MA.** 2016. Zika Virus. N Engl J Med **374:**1552-1563.

2. **Talero-Gutierrez C, Rivera-Molina A, Perez-Pavajeau C, Ossa-Ospina I, Santos-Garcia C, Rojas-Anaya MC, de-la-Torre A.** 2018. Zika virus epidemiology: from Uganda to world pandemic, an update. Epidemiol Infect doi:10.1017/s0950268818000419**:**1-7.

3. **Cao-Lormeau VM, Blake A, Mons S, Lastere S, Roche C, Vanhomwegen J, Dub T, Baudouin L, Teissier A, Larre P, Vial AL, Decam C, Choumet V, Halstead SK, Willison HJ, Musset L, Manuguerra JC, Despres P, Fournier E, Mallet HP, Musso D, Fontanet A, Neil J, Ghawche F.** 2016. Guillain-Barre Syndrome outbreak associated with Zika virus infection in French Polynesia: a case-control study. Lancet **387:**1531-1539.

4. **Munoz LS, Parra B, Pardo CA.** 2017. Neurological Implications of Zika Virus Infection in Adults. J Infect Dis **216:**S897-s905.

5. **Rasmussen SA, Jamieson DJ, Honein MA, Petersen LR.** 2016. Zika Virus and Birth Defects--Reviewing the Evidence for Causality. N Engl J Med **374:**1981-1987.

6. **Sanz Cortes M, Rivera AM, Yepez M, Guimaraes CV, Diaz Yunes I, Zarutskie A, Davila I, Shetty A, Mahadev A, Serrano SM, Castillo N, Lee W, Valentine G, Belfort M, Parra G, Mohila C, Aagaard K, Parra M.** 2018. Clinical Assessment and Brain Findings in a Cohort of Mothers, Fetuses and Infants Infected with Zika Virus. Am J Obstet Gynecol doi:10.1016/j.ajog.2018.01.012.

7. **Xia H, Luo H, Shan C, Muruato AE, Nunes BTD, Medeiros DBA, Zou J, Xie X, Giraldo MI, Vasconcelos PFC, Weaver SC, Wang T, Rajsbaum R, Shi PY.** 2018. An

33

688   evolutionary NS1 mutation enhances Zika virus evasion of host interferon induction. Nat

689   Commun **9:**414.

690   8.   **Liu Y, Liu J, Du S, Shan C, Nie K, Zhang R, Li XF, Zhang R, Wang T, Qin CF,**

691   **Wang P, Shi PY, Cheng G.** 2017. Evolutionary enhancement of Zika virus infectivity in

692   Aedes aegypti mosquitoes. Nature **545:**482-486.

693   9.   **Flamand C, Fritzell C, Matheus S, Dueymes M, Carles G, Favre A, Enfissi A, Adde**

694   **A, Demar M, Kazanji M, Cauchemez S, Rousset D.** 2017. The proportion of

695   asymptomatic infections and spectrum of disease among pregnant women infected by

696   Zika virus: systematic monitoring in French Guiana, 2016. Euro Surveill **22**.

697   10.   **Cauchemez S, Besnard M, Bompard P, Dub T, Guillemette-Artur P, Eyrolle-**

698   **Guignot D, Salje H, Van Kerkhove MD, Abadie V, Garel C, Fontanet A, Mallet HP.**

699   2016. Association between Zika virus and microcephaly in French Polynesia, 2013-15: a

700   retrospective study. Lancet **387:**2125-2132.

701   11.   **Brasil P, Pereira JP, Jr., Moreira ME, Ribeiro Nogueira RM, Damasceno L,**

702   **Wakimoto M, Rabello RS, Valderramos SG, Halai UA, Salles TS, Zin AA, Horovitz**

703   **D, Daltro P, Boechat M, Raja Gabaglia C, Carvalho de Sequeira P, Pilotto JH,**

704   **Medialdea-Carrera R, Cotrim da Cunha D, Abreu de Carvalho LM, Pone M,**

705   **Machado Siqueira A, Calvet GA, Rodrigues Baiao AE, Neves ES, Nassar de**

706   **Carvalho PR, Hasue RH, Marschik PB, Einspieler C, Janzen C, Cherry JD, Bispo**

707   **de Filippis AM, Nielsen-Saines K.** 2016. Zika Virus Infection in Pregnant Women in

708   Rio de Janeiro. N Engl J Med **375:**2321-2334.

709   12.   **McGrath EL, Rossi SL, Gao J, Widen SG, Grant AC, Dunn TJ, Azar SR, Roundy**

710   **CM, Xiong Y, Prusak DJ, Loucas BD, Wood TG, Yu Y, Fernandez-Salas I, Weaver**

711   **SC, Vasilakis N, Wu P.** 2017. Differential Responses of Human Fetal Brain Neural Stem

712   Cells to Zika Virus Infection. Stem Cell Reports doi:10.1016/j.stemcr.2017.01.008.

713   13.   **Caires-Junior LC, Goulart E, Melo US, Araujo BSH, Alvizi L, Soares-Schanoski A,**

714   **de Oliveira DF, Kobayashi GS, Griesi-Oliveira K, Musso CM, Amaral MS, daSilva**

715   **LF, Astray RM, Suarez-Patino SF, Ventini DC, Gomes da Silva S, Yamamoto GL,**

716   **Ezquina S, Naslavsky MS, Telles-Silva KA, Weinmann K, van der Linden V, van**

717   **der Linden H, de Oliveira JMR, Arrais NRM, Melo A, Figueiredo T, Santos S,**

718   **Meira JCG, Passos SD, de Almeida RP, Bispo AJB, Cavalheiro EA, Kalil J, Cunha-**

719   **Neto E, Nakaya H, Andreata-Santos R, de Souza Ferreira LC, Verjovski-Almeida S,**

720   **Ho PL, Passos-Bueno MR, Zatz M.** 2018. Discordant congenital Zika syndrome twins

721   show differential in vitro viral susceptibility of neural progenitor cells. Nat Commun

722   **9:**475.

723   14.   **Julander JG, Siddharthan V.** 2017. Small-Animal Models of Zika Virus. J Infect Dis

724   **216:**S919-s927.

725   15.   **Winkler CW, Peterson KE.** 2017. Using immunocompromised mice to identify

726   mechanisms of Zika virus transmission and pathogenesis. Immunology

727   doi:10.1111/imm.12883.

728   16.   **Li H, Saucedo-Cuevas L, Regla-Nava JA, Chai G, Sheets N, Tang W, Terskikh AV,**

729   **Shresta S, Gleeson JG.** 2016. Zika Virus Infects Neural Progenitors in the Adult Mouse

730   Brain and Alters Proliferation. Cell Stem Cell doi:10.1016/j.stem.2016.08.005.

731   17.   **Rosenfeld AB, Doobin DJ, Warren AL, Racaniello VR, Vallee RB.** 2017. Replication

732   of early and recent Zika virus isolates throughout mouse brain development. Proc Natl

733   Acad Sci U S A doi:10.1073/pnas.1714624114.

734   18.   **Tang WW, Young MP, Mamidi A, Regla-Nava JA, Kim K, Shresta S.** 2016. A

735   Mouse Model of Zika Virus Sexual Transmission and Vaginal Viral Replication. Cell

736   Rep **17:**3091-3098.

737   19.   **Duggal NK, McDonald EM, Ritter JM, Brault AC.** 2018. Sexual transmission of Zika

738   virus enhances in utero transmission in a mouse model. Sci Rep **8:**4510.

739   20.   **Winkler CW, Woods TA, Rosenke R, Scott DP, Best SM, Peterson KE.** 2017. Sexual

740   and Vertical Transmission of Zika Virus in anti-interferon receptor-treated Rag1-

741   deficient mice. Sci Rep **7:**7176.

742   21.   **Jaeger AS, Murrieta RA, Goren LR, Crooks CM, Moriarty RV, Weiler AM,**

743   **Rybarczyk S, Semler MR, Huffman C, Mejia A, Simmons HA, Fritsch M, Osorio**

744   **JE, Eickhoff JC, O'Connor SL, Ebel GD, Friedrich TC, Aliota MT.** 2019. Zika

745   viruses of African and Asian lineages cause fetal harm in a mouse model of vertical

746   transmission. PLoS Negl Trop Dis **13:**e0007343.

747   22.   **Yockey LJ, Varela L, Rakib T, Khoury-Hanold W, Fink SL, Stutz B, Szigeti-Buck**

748   **K, Van den Pol A, Lindenbach BD, Horvath TL, Iwasaki A.** 2016. Vaginal Exposure

749   to Zika Virus during Pregnancy Leads to Fetal Brain Infection. Cell **166:**1247-

750   1256.e1244.

751   23.   **Miner JJ, Cao B, Govero J, Smith AM, Fernandez E, Cabrera OH, Garber C, Noll**

752   **M, Klein RS, Noguchi KK, Mysorekar IU, Diamond MS.** 2016. Zika Virus Infection

753   during Pregnancy in Mice Causes Placental Damage and Fetal Demise. Cell **165:**1081-

754   1091.

755   24.   **Paul AM, Acharya D, Neupane B, Thompson EA, Gonzalez-Fernandez G, Copeland**

756   **KM, Garrett M, Liu H, Lopez ME, de Cruz M, Flynt A, Liao J, Guo YL, Gonzalez-**

757   **Fernandez F, Vig PJS, Bai F.** 2018. Congenital Zika Virus Infection in

36

758   Immunocompetent Mice Causes Postnatal Growth Impediment and Neurobehavioral

759   Deficits. Front Microbiol **9:**2028.

760   25.   **Caine EA, Jagger BW, Diamond MS.** 2018. Animal Models of Zika Virus Infection

761   during Pregnancy. Viruses **10**.

762   26.   **Wu Y, Liu Q, Zhou J, Xie W, Chen C, Wang Z, Yang H, Cui J.** 2017. Zika virus

763   evades interferon-mediated antiviral response through the co-operation of multiple

764   nonstructural proteins in vitro. Cell Discov **3:**17006.

765   27.   **Pierson TC, Diamond MS.** 2018. The emergence of Zika virus and its new clinical

766   syndromes. Nature **560:**573-581.

767   28.   **Grant A, Ponia SS, Tripathi S, Balasubramaniam V, Miorin L, Sourisseau M,**

768   **Schwarz MC, Sanchez-Seco MP, Evans MJ, Best SM, Garcia-Sastre A.** 2016. Zika

769   Virus Targets Human STAT2 to Inhibit Type I Interferon Signaling. Cell Host Microbe

770   **19:**882-890.

771   29.   **Lazear HM, Govero J, Smith AM, Platt DJ, Fernandez E, Miner JJ, Diamond MS.**

772   2016. A Mouse Model of Zika Virus Pathogenesis. Cell Host Microbe **19:**720-730.

773   30.   **Sheehan KC, Lai KS, Dunn GP, Bruce AT, Diamond MS, Heutel JD, Dungo-Arthur**

774   **C, Carrero JA, White JM, Hertzog PJ, Schreiber RD.** 2006. Blocking monoclonal

775   antibodies specific for mouse IFN-alpha/beta receptor subunit 1 (IFNAR-1) from mice

776   immunized by in vivo hydrodynamic transfection. J Interferon Cytokine Res **26:**804-819.

777   31.   **Smith DR, Hollidge B, Daye S, Zeng X, Blancett C, Kuszpit K, Bocan T, Koehler**

778   **JW, Coyne S, Minogue T, Kenny T, Chi X, Yim S, Miller L, Schmaljohn C, Bavari**

779   **S, Golden JW.** 2017. Neuropathogenesis of Zika Virus in a Highly Susceptible

780   Immunocompetent Mouse Model after Antibody Blockade of Type I Interferon. PLoS

781   Negl Trop Dis **11:**e0005296.

782   32.   **Kamiyama N, Soma R, Hidano S, Watanabe K, Umekita H, Fukuda C, Noguchi K,**

783   **Gendo Y, Ozaki T, Sonoda A, Sachi N, Runtuwene LR, Miura Y, Matsubara E,**

784   **Tajima S, Takasaki T, Eshita Y, Kobayashi T.** 2017. Ribavirin inhibits Zika virus

785   (ZIKV) replication in vitro and suppresses viremia in ZIKV-infected STAT1-deficient

786   mice. Antiviral Res doi:10.1016/j.antiviral.2017.08.007.

787   33.   **Jagger BW, Miner JJ, Cao B, Arora N, Smith AM, Kovacs A, Mysorekar IU, Coyne**

788   **CB, Diamond MS.** 2017. Gestational Stage and IFN-lambda Signaling Regulate ZIKV

789   Infection In Utero. Cell Host Microbe **22:**366-376.e363.

790   34.   **Tripathi S, Balasubramaniam VR, Brown JA, Mena I, Grant A, Bardina SV,**

791   **Maringer K, Schwarz MC, Maestre AM, Sourisseau M, Albrecht RA, Krammer F,**

792   **Evans MJ, Fernandez-Sesma A, Lim JK, Garcia-Sastre A.** 2017. A novel Zika virus

793   mouse model reveals strain specific differences in virus pathogenesis and host

794   inflammatory immune responses. PLoS Pathog **13:**e1006258.

795   35.   **Manet C, Roth C, Tawfik A, Cantaert T, Sakuntabhai A, Montagutelli X.** 2018. Host

796   genetic control of mosquito-borne Flavivirus infections. Mamm Genome

797   doi:10.1007/s00335-018-9775-2.

798   36.   **Snyder-Keller A, Kramer L, Zink S, Bolivar VJ.** 2019. Mouse strain and sex-

799   dependent differences in long-term behavioral abnormalities and neuropathologies after

800   developmental zika infection. J Neurosci doi:10.1523/jneurosci.2666-18.2019.

801   37.   **Saul MC, Philip VM, Reinholdt LG, Chesler EJ.** 2019. High-Diversity Mouse

802   Populations for Complex Traits. Trends in Genetics doi:10.1016/j.tig.2019.04.003.

803   38.   **Montagutelli X.** 2000. Effect of the genetic background on the phenotype of mouse

804   mutations. J Am Soc Nephrol **11 Suppl 16:**S101-105.

805   39.   **Nadeau JH.** 2001. Modifier genes in mice and humans. Nat Rev Genet **2:**165-174.

38

806   40.   **Consortium.** 2012. The genome architecture of the Collaborative Cross mouse genetic

807   reference population. Genetics **190:**389-401.

808   41.   **Roberts A, Pardo-Manuel de Villena F, Wang W, McMillan L, Threadgill DW.**

809   2007. The polymorphism architecture of mouse genetic resources elucidated using

810   genome-wide resequencing data: implications for QTL discovery and systems genetics.

811   Mamm Genome **18:**473-481.

812   42.   **Keane TM, Goodstadt L, Danecek P, White MA, Wong K, Yalcin B, Heger A, Agam**

813   **A, Slater G, Goodson M, Furlotte NA, Eskin E, Nellaker C, Whitley H, Cleak J,**

814   **Janowitz D, Hernandez-Pliego P, Edwards A, Belgard TG, Oliver PL, McIntyre RE,**

815   **Bhomra A, Nicod J, Gan X, Yuan W, van der Weyden L, Steward CA, Bala S,**

816   **Stalker J, Mott R, Durbin R, Jackson IJ, Czechanski A, Guerra-Assuncao JA,**

817   **Donahue LR, Reinholdt LG, Payseur BA, Ponting CP, Birney E, Flint J, Adams DJ.**

818   2011. Mouse genomic variation and its effect on phenotypes and gene regulation. Nature

819   **477:**289-294.

820   43.   **Rasmussen AL, Okumura A, Ferris MT, Green R, Feldmann F, Kelly SM, Scott DP,**

821   **Safronetz D, Haddock E, LaCasse R, Thomas MJ, Sova P, Carter VS, Weiss JM,**

822   **Miller DR, Shaw GD, Korth MJ, Heise MT, Baric RS, de Villena FP, Feldmann H,**

823   **Katze MG.** 2014. Host genetic diversity enables Ebola hemorrhagic fever pathogenesis

824   and resistance. Science **346:**987-991.

825   44.   **Gralinski LE, Ferris MT, Aylor DL, Whitmore AC, Green R, Frieman MB, Deming**

826   **D, Menachery VD, Miller DR, Buus RJ, Bell TA, Churchill GA, Threadgill DW,**

827   **Katze MG, McMillan L, Valdar W, Heise MT, Pardo-Manuel de Villena F, Baric**

828   **RS.** 2015. Genome Wide Identification of SARS-CoV Susceptibility Loci Using the

829   Collaborative Cross. PLoS Genet **11:**e1005504.

830   45.   **Graham JB, Thomas S, Swarts J, McMillan AA, Ferris MT, Suthar MS, Treuting**

831   **PM, Ireton R, Gale M, Jr., Lund JM.** 2015. Genetic diversity in the collaborative cross

832   model recapitulates human West Nile virus disease outcomes. MBio **6:**e00493-00415.

833   46.   **Graham JB, Swarts JL, Wilkins C, Thomas S, Green R, Sekine A, Voss KM, Ireton**

834   **RC, Mooney M, Choonoo G, Miller DR, Treuting PM, Pardo Manuel de Villena F,**

835   **Ferris MT, McWeeney S, Gale M, Jr., Lund JM.** 2016. A Mouse Model of Chronic

836   West Nile Virus Disease. PLoS Pathog **12:**e1005996.

837   47.   **Green R, Wilkins C, Thomas S, Sekine A, Hendrick DM, Voss K, Ireton RC,**

838   **Mooney M, Go JT, Choonoo G, Jeng S, de Villena FP, Ferris MT, McWeeney S,**

839   **Gale M, Jr.** 2017. Oas1b-dependent Immune Transcriptional Profiles of West Nile Virus

840   Infection in the Collaborative Cross. G3 (Bethesda) **7:**1665-1682.

841   48.   **Bottomly D, Ferris MT, Aicher LD, Rosenzweig E, Whitmore A, Aylor DL,**

842   **Haagmans BL, Gralinski LE, Bradel-Tretheway BG, Bryan JT, Threadgill DW, de**

843   **Villena FP, Baric RS, Katze MG, Heise M, McWeeney SK.** 2012. Expression

844   quantitative trait Loci for extreme host response to influenza a in pre-collaborative cross

845   mice. G3 (Bethesda) **2:**213-221.

846   49.   **Elbahesh H, Schughart K.** 2016. Genetically diverse CC-founder mouse strains

847   replicate the human influenza gene expression signature. Sci Rep **6:**26437.

848   50.   **Ferris MT, Aylor DL, Bottomly D, Whitmore AC, Aicher LD, Bell TA, Bradel-**

849   **Tretheway B, Bryan JT, Buus RJ, Gralinski LE, Haagmans BL, McMillan L, Miller**

850   **DR, Rosenzweig E, Valdar W, Wang J, Churchill GA, Threadgill DW, McWeeney**

851   **SK, Katze MG, Pardo-Manuel de Villena F, Baric RS, Heise MT.** 2013. Modeling

852   host genetic regulation of influenza pathogenesis in the collaborative cross. PLoS Pathog

853   **9:**e1003196.

854   51.   **Lore NI, Iraqi FA, Bragonzi A.** 2015. Host genetic diversity influences the severity of

855   Pseudomonas aeruginosa pneumonia in the Collaborative Cross mice. BMC Genet

856   **16:**106.

857   52.   **Zhang J, Malo D, Mott R, Panthier JJ, Montagutelli X, Jaubert J.** 2018.

858   Identification of new loci involved in the host susceptibility to Salmonella Typhimurium

859   in collaborative cross mice. BMC Genomics **19:**303.

860   53.   **Durrant C, Tayem H, Yalcin B, Cleak J, Goodstadt L, de Villena FP, Mott R, Iraqi**

861   **FA.** 2011. Collaborative Cross mice and their power to map host susceptibility to

862   Aspergillus fumigatus infection. Genome Res **21:**1239-1248.

863   54.   **Noll KE, Ferris MT, Heise MT.** 2019. The Collaborative Cross: A Systems Genetics

864   Resource for Studying Host-Pathogen Interactions. Cell Host Microbe **25:**484-498.

865   55.   **Rossi SL, Tesh RB, Azar SR, Muruato AE, Hanley KA, Auguste AJ, Langsjoen RM,**

866   **Paessler S, Vasilakis N, Weaver SC.** 2016. Characterization of a Novel Murine Model

867   to Study Zika Virus. Am J Trop Med Hyg **94:**1362-1369.

868   56.   **Dowall SD, Graham VA, Rayner E, Hunter L, Atkinson B, Pearson G, Dennis M,**

869   **Hewson R.** 2017. Lineage-dependent differences in the disease progression of Zika virus

870   infection in type-I interferon receptor knockout (A129) mice. PLoS Negl Trop Dis

871   **11:**e0005704.

872   57.   **Srivastava A, Morgan AP, Najarian ML, Sarsani VK, Sigmon JS, Shorter JR,**

873   **Kashfeen A, McMullan RC, Williams LH, Giusti-Rodriguez P, Ferris MT, Sullivan**

874   **P, Hock P, Miller DR, Bell TA, McMillan L, Churchill GA, de Villena FP.** 2017.

875   Genomes of the Mouse Collaborative Cross. Genetics **206:**537-556.

876   58.   **Liang H, Yang R, Liu Z, Li M, Liu H, Jin X.** 2018. Recombinant Zika virus envelope

877   protein elicited protective immunity against Zika virus in immunocompetent mice. PLoS

878   One **13:**e0194860.

879   59.   **Rutledge H, Aylor DL, Carpenter DE, Peck BC, Chines P, Ostrowski LE, Chesler**

880   **EJ, Churchill GA, de Villena FP, Kelada SN.** 2014. Genetic regulation of Zfp30,

881   CXCL1, and neutrophilic inflammation in murine lung. Genetics **198:**735-745.

882   60.   **Mashimo T, Lucas M, Simon-Chazottes D, Frenkiel MP, Montagutelli X, Ceccaldi**

883   **PE, Deubel V, Guenet JL, Despres P.** 2002. A nonsense mutation in the gene encoding

884   2'-5'-oligoadenylate synthetase/L1 isoform is associated with West Nile virus

885   susceptibility in laboratory mice. Proc Natl Acad Sci U S A **99:**11311-11316.

886   61.   **Govero J, Esakky P, Scheaffer SM, Fernandez E, Drury A, Platt DJ, Gorman MJ,**

887   **Richner JM, Caine EA, Salazar V, Moley KH, Diamond MS.** 2016. Zika virus

888   infection damages the testes in mice. Nature **540:**438-442.

889   62.   **Manangeeswaran M, Ireland DD, Verthelyi D.** 2016. Zika (PRVABC59) Infection Is

890   Associated with T cell Infiltration and Neurodegeneration in CNS of Immunocompetent

891   Neonatal C57Bl/6 Mice. PLoS pathogens **12:**e1006004.

892   63.   **van den Pol AN, Mao G, Yang Y, Ornaghi S, Davis JN.** 2017. Zika Virus Targeting in

893   the Developing Brain. J Neurosci **37:**2161-2175.

894   64.   **Li S, Armstrong N, Zhao H, Hou W, Liu J, Chen C, Wan J, Wang W, Zhong C, Liu**

895   **C, Zhu H, Xia N, Cheng T, Tang Q.** 2018. Zika Virus Fatally Infects Wild Type

896   Neonatal Mice and Replicates in Central Nervous System. Viruses **10.**

897   65.   **Gorman MJ, Caine EA, Zaitsev K, Begley MC, Weger-Lucarelli J, Uccellini MB,**

898   **Tripathi S, Morrison J, Yount BL, Dinnon KH, 3rd, Ruckert C, Young MC, Zhu Z,**

899   **Robertson SJ, McNally KL, Ye J, Cao B, Mysorekar IU, Ebel GD, Baric RS, Best**

900   **SM, Artyomov MN, Garcia-Sastre A, Diamond MS.** 2018. An Immunocompetent

901   Mouse Model of Zika Virus Infection. Cell Host Microbe **23:**672-685.e676.

902 66. **Manet C, Roth C, Tawfik A, Cantaert T, Sakuntabhai A, Montagutelli X.** 2018. Host

903   genetic control of mosquito-borne Flavivirus infections. Mamm Genome **29:**384-407.

904 67. **Samuel MA, Diamond MS.** 2005. Alpha/beta interferon protects against lethal West

905   Nile virus infection by restricting cellular tropism and enhancing neuronal survival. J

906   Virol **79:**13350-13361.

907 68. **Churchill GA, Airey DC, Allayee H, Angel JM, Attie AD, Beatty J, Beavis WD,**

908   **Belknap JK, Bennett B, Berrettini W, Bleich A, Bogue M, Broman KW, Buck KJ,**

909   **Buckler E, Burmeister M, Chesler EJ, Cheverud JM, Clapcote S, Cook MN, Cox**

910   **RD, Crabbe JC, Crusio WE, Darvasi A, Deschepper CF, Doerge RW, Farber CR,**

911   **Forejt J, Gaile D, Garlow SJ, Geiger H, Gershenfeld H, Gordon T, Gu J, Gu W, de**

912   **Haan G, Hayes NL, Heller C, Himmelbauer H, Hitzemann R, Hunter K, Hsu HC,**

913   **Iraqi FA, Ivandic B, Jacob HJ, Jansen RC, Jepsen KJ, Johnson DK, Johnson TE,**

914   **Kempermann G, et al.** 2004. The Collaborative Cross, a community resource for the

915   genetic analysis of complex traits. Nat Genet **36:**1133-1137.

916 69. **Duffy MR, Chen TH, Hancock WT, Powers AM, Kool JL, Lanciotti RS, Pretrick M,**

917   **Marfel M, Holzbauer S, Dubray C, Guillaumot L, Griggs A, Bel M, Lambert AJ,**

918   **Laven J, Kosoy O, Panella A, Biggerstaff BJ, Fischer M, Hayes EB.** 2009. Zika virus

919   outbreak on Yap Island, Federated States of Micronesia. The New England journal of

920   medicine **360:**2536-2543.

921 70. **Aliota MT, Caine EA, Walker EC, Larkin KE, Camacho E, Osorio JE.** 2016.

922   Characterization of Lethal Zika Virus Infection in AG129 Mice. PLoS Negl Trop Dis

923   **10:**e0004682.

71. **Dowall SD, Graham VA, Rayner E, Atkinson B, Hall G, Watson RJ, Bosworth A, Bonney LC, Kitchen S, Hewson R.** 2016. A Susceptible Mouse Model for Zika Virus Infection. PLoS neglected tropical diseases **10:**e0004658.

72. **Noll KE, Ferris MT, Heise MT.** 2019. The Collaborative Cross: A Systems Genetics Resource for Studying Host-Pathogen Interactions. Cell Host & Microbe **25:**484-498.

73. **do Valle TZ, Billecocq A, Guillemot L, Alberts R, Gommet C, Geffers R, Calabrese K, Schughart K, Bouloy M, Montagutelli X, Panthier JJ.** 2010. A new mouse model reveals a critical role for host innate immunity in resistance to Rift Valley fever. J Immunol **185:**6146-6156.

74. **Le-Trilling VT, Trilling M.** 2017. Mouse newborn cells allow highly productive mouse cytomegalovirus replication, constituting a novel convenient primary cell culture system. PLoS One **12:**e0174695.

75. **Setoh YX, Peng NY, Nakayama E, Amarilla AA, Prow NA, Suhrbier A, Khromykh AA.** 2018. Fetal Brain Infection Is Not a Unique Characteristic of Brazilian Zika Viruses. Viruses **10**.

76. **Savidis G, Perreira JM, Portmann JM, Meraner P, Guo Z, Green S, Brass AL.** 2016. The IFITMs Inhibit Zika Virus Replication. Cell Rep **15:**2323-2330.

77. **Lang J, Cheng Y, Rolfe A, Hammack C, Vera D, Kyle K, Wang J, Meissner TB, Ren Y, Cowan C, Tang H.** 2018. An hPSC-Derived Tissue-Resident Macrophage Model Reveals Differential Responses of Macrophages to ZIKV and DENV Infection. Stem Cell Reports **11:**348-362.

78. **Pachulec E, Abdelwahed Bagga RB, Chevallier L, O'Donnell H, Guillas C, Jaubert J, Montagutelli X, Carniel E, Demeure CE.** 2017. Enhanced Macrophage M1

947   Polarization and Resistance to Apoptosis Enable Resistance to Plague. J Infect Dis

948   **216:**761-770.

949   79.   **Horisberger MA, Staeheli P, Haller O.** 1983. Interferon induces a unique protein in

950   mouse cells bearing a gene for resistance to influenza virus. Proc Natl Acad Sci U S A

951   **80:**1910-1914.

952   80.   **Keele GR, Crouse WL, Kelada SNP, Valdar W.** 2019. Determinants of QTL Mapping

953   Power in the Realized Collaborative Cross. G3 (Bethesda) doi:10.1534/g3.119.400194.

954   81.   **Simon-Loriere E, Lin RJ, Kalayanarooj SM, Chuansumrit A, Casademont I, Lin**

955   **SY, Yu HP, Lert-Itthiporn W, Chaiyaratana W, Tangthawornchaikul N,**

956   **Tangnararatchakit K, Vasanawathana S, Chang BL, Suriyaphol P, Yoksan S,**

957   **Malasit P, Despres P, Paul R, Lin YL, Sakuntabhai A.** 2015. High Anti-Dengue Virus

958   Activity of the OAS Gene Family Is Associated With Increased Severity of Dengue. J

959   Infect Dis **212:**2011-2020.

960   82.   **Welsh CE, Miller DR, Manly KF, Wang J, McMillan L, Morahan G, Mott R, Iraqi**

961   **FA, Threadgill DW, de Villena FP.** 2012. Status and access to the Collaborative Cross

962   population. Mamm Genome **23:**706-712.

963   83.   **Fansiri T, Fontaine A, Diancourt L, Caro V, Thaisomboonsuk B, Richardson JH,**

964   **Jarman RG, Ponlawat A, Lambrechts L.** 2013. Genetic mapping of specific

965   interactions between Aedes aegypti mosquitoes and dengue viruses. PLoS Genet

966   **9:**e1003621.

967   84.   **Tokuda S, Do Valle TZ, Batista L, Simon-Chazottes D, Guillemot L, Bouloy M,**

968   **Flamand M, Montagutelli X, Panthier JJ.** 2015. The genetic basis for susceptibility to

969   Rift Valley fever disease in MBT/Pas mice. Genes Immun **16:**206-212.

970   85.   **Sheehan KC, Lazear HM, Diamond MS, Schreiber RD.** 2015. Selective Blockade of

971   Interferon-alpha and -beta Reveals Their Non-Redundant Functions in a Mouse Model of

972   West Nile Virus Infection. PLoS One **10:**e0128636.

973   86.   **Shimizu S.** 2004. CHAPTER 32 - Routes of Administration, p 527-542. *In* Hedrich HJ,

974   Bullock G (ed), The Laboratory Mouse doi:https://doi.org/10.1016/B978-012336425-

975   8/50085-6. Academic Press, London.

976   87.   **Lanciotti RS, Kosoy OL, Laven JJ, Velez JO, Lambert AJ, Johnson AJ, Stanfield**

977   **SM, Duffy MR.** 2008. Genetic and serologic properties of Zika virus associated with an

978   epidemic, Yap State, Micronesia, 2007. Emerg Infect Dis **14:**1232-1239.

979   88.   **Faye O, Faye O, Diallo D, Diallo M, Weidmann M, Sall AA.** 2013. Quantitative real-

980   time PCR detection of Zika virus and evaluation with field-caught mosquitoes. Virol J

981   **10:**311.

982   89.   **Fontaine A, Jiolle D, Moltini-Conclois I, Lequime S, Lambrechts L.** 2016. Excretion

983   of dengue virus RNA by Aedes aegypti allows non-destructive monitoring of viral

984   dissemination in individual mosquitoes. Sci Rep **6:**24885.

985   90.   **Verdonk F, Roux P, Flamant P, Fiette L, Bozza FA, Simard S, Lemaire M, Plaud B,**

986   **Shorte SL, Sharshar T, Chretien F, Danckaert A.** 2016. Phenotypic clustering: a novel

987   method for microglial morphology analysis. J Neuroinflammation **13:**153.

988   91.   **Broman KW, Gatti DM, Simecek P, Furlotte NA, Prins P, Sen S, Yandell BS,**

989   **Churchill GA.** 2019. R/qtl2: Software for Mapping Quantitative Trait Loci with High-

990   Dimensional Data and Multiparent Populations. Genetics **211:**495-502.

991

992

46

993

FIGURE LEGENDS

FIG 1 ZIKV disease severity in *Ifnar1*-deficient mice is driven by the genetic background.

6-7 week-old 129-*Ifnar1* (n = 7) and B6-*Ifnar1* (n = 10) mice were infected IP with 10^7 FFUs of ZIKV FG15 and monitored for 14 days. (A) Average clinical score, with numerical values given as follows: 0, no symptom; 1, ruffled fur; 2, emaciation, hunched posture and/or hypo activity; 3, hind limb weakness, prostration and/or closed eyes; and 4, moribund or dead. (B) Kaplan-Meier survival curves showing 100% lethality in B6-*Ifnar1* mice at day 7 p.i. and survival of 6/7 129-*Ifnar1* mice (logrank test, *** : p = 0.0002). B6-*Ifnar1* mice developed early symptoms which rapidly evolved to death, while 129-*Ifnar1* mice developed symptoms two days later which eventually resolved in most mice.

FIG 2 Establishment and validation of the experimental conditions for assessing susceptibility to ZIKV in CC strains. (A) The efficacy of the MAR1-5A3 mAb to block the IFNAR receptor in diverse mouse genetic backgrounds was determined by Western blotting on mouse embryonic fibroblasts (MEFs) derived from C57BL/6J, CC001 and CC071 strains. The phosphorylation of STAT1 was equally induced by IFN-α stimulation and fully inhibited by the MAR1-5A3 mAb in the three strains, as in the untreated and unstimulated CD-1 MEFs. (B) When treated with MAR1-5A3 24h prior to ZIKV infection (filled circles), mice of both CC001 and CC071 strains (n = 9 and 8, respectively) were much more permissive to viral replication with 4 to 5 $\log_{10}$ times more copies of viral genome than mice without treatment (open circles; n = 3 and 2, respectively) throughout the first three days p.i. ("x" denotes a sample below the detection level). (C) The kinetics of plasma viral load in 129-*Ifnar1* and 4 CC strains showed a maximum in most individuals at day 2 p.i. which was subsequently selected to measure peak viral load in all CC

1016   strains. Each circle represents a mouse analyzed on days 1, 2, 3 and 6. (D) Correlation between

1017   plasma viral load determined by FFA (x-axis) and RT-qPCR (y-axis) was established on 46

1018   blood samples from 129-*Ifnar1*, B6-*Ifnar1* and 10 CC strains (circles show the mean of each

1019   strain; the number of mice per strain is shown in parentheses). The two variables were strongly

1020   correlated over a 3 $\log_{10}$ range of viral genome copies ($r^2 = 0.89$, $p = 9.9 \times 10^{-17}$), the number of

1021   genome copies by RT-qPCR being on average 3 $\log_{10}$ units higher than the viral titer by FFA. (E)

1022   Plasma viral load at day 2 p.i. was not significantly different ($p = 0.24$) between males and

1023   females of 129-*Ifnar1* and 4 CC strains for which age-matched mice of both sexes had been

1024   tested (with $n \geq 4$ mice per group).

1025   **FIG 3** CC genetic diversity strongly impacts clinical severity and plasma viral load. Thirty-five

1026   CC strains ($n = 2$ to 9 per strain) were infected IP with 10^7 FFUs of ZIKV FG15, 24hr after IP

1027   injection of 2 mg of MAR1-5A3 mAb. 129-*Ifnar1* ($n = 24$) and B6-*Ifnar1* ($n = 5$) mice were

1028   similarly infected without mAb treatment. (A) Clinical scores at day 7 p.i. as the percentage of

1029   mice in the five levels of severity (same as in FIG 1). Most CC strains did not show any

1030   symptoms, while 78% (7/9) of CC071 died before day 8 p.i. (B) Plasma viral load at days 2

1031   (upper values) and 6 p.i. (lower values) quantified by RT-qPCR, shown as box-whisker plot with

1032   outliers as dots (strains are shown in the same order as in A). CC genetic background had a

1033   highly significant effect on viral load at day 2 p.i. (Kruskal-Wallis, $p = 4.8 \times 10^{-15}$) and day 6 p.i.

1034   (Kruskal-Wallis, $p = 1.1 \times 10^{-10}$). (C) Difference between plasma viral loads at days 2 and 6 p.i.

1035   Strains are sorted by increasing absolute difference, therefore in a different order from A and B.

1036   CC genetic background had a highly significant effect on viral load decrease (Kruskal-Wallis, p

1037 $= 2.2 \times 10^{-12}$). Likewise, viral load decreased much faster in 129-*Ifnar1* than in B6-*Ifnar1* mice

48

1038 (Wilcoxon, *** : p = $1.7\mathrm{x}10^{-5}$). (B and C) Arrows indicate the subset of CC mouse strains

1039 selected for detailed study.

1040 **FIG 4** The differences in susceptibility to ZIKV between CC strains are conserved with other

1041 flaviviruses. (A) Mice from three selected CC strains treated with MAR1-5A3 mAb and 129-

1042 *Ifnar1* mice were infected intraperitoneally with 10^3 FFUs of ZIKV HD78788. Left : average

1043 clinical score, with numerical values given as in FIG 1. CC071 and 129-*Ifnar1* mice rapidly

1044 developed severe symptoms and died while CC001 and CC005 mice were mostly resistant.

1045 Center : Kaplan-Meier survival curves (logrank test). Right : plasma viral load at day 2 p.i.,

1046 measured by RT-qPCR and expressed as ZIKV genome copies per milliliter, was much lower in

1047 CC001 than in the two other CC strains (Wilcoxon). (B) Viral load after ZIKV infection (left,

1048 data extracted from FIG 3) and DENV infection (right, IV infection with 2.10^6 FFUs of DENV

1049 KDH0026A) was compared in mAb-treated CC001, CC071 and B6 mice and in 129-*Ifnar1* and

1050 B6-*Ifnar1*. Most between-strain differences were conserved between the two viruses (*t* test). (C)

1051 Left : Kaplan-Meier survival curves of four male mice of each of the three selected CC strains

1052 infected IP with 1000 FFU of WNV strain IS-98-ST1 and monitored for 14 days. CC071 died

1053 earlier than CC005 and CC001 mice (logrank test). Right : Kaplan-Meier survival curves of four

1054 to five male mice of BALB/cByJ and each of the three selected CC strains infected IP with100

1055 PFUs of RVFV strain ZH548 and monitored for 14 days. No significant difference was found

1056 among the three CC strains and only CC001 mice survived longer than BALB/c mice (logrank

1057 test, p > 0.05). * p < 0.05; ** p < 0.01; *** p < 0.001.

1058 **FIG 5** Genetic analysis of susceptibility to ZIKV fails to identify simple genetic control.

1059 Genome-wide linkage analysis for the plasma viral load at day 2 p.i.(A), the plasma viral load at

1060 day 6 p.i. (B) and the decrease rate of plasma viral load (C) on the 35 CC strains shown on FIG

49

1061   3. The x-axis represents genomic location; the y-axis is the LOD score, representing the

1062   statistical association between the phenotype and the genomic location. Genome-wide thresholds

1063   p = 0.1, p=0.05 and p = 0.01, computed from 1000 permutations, are represented by dashed

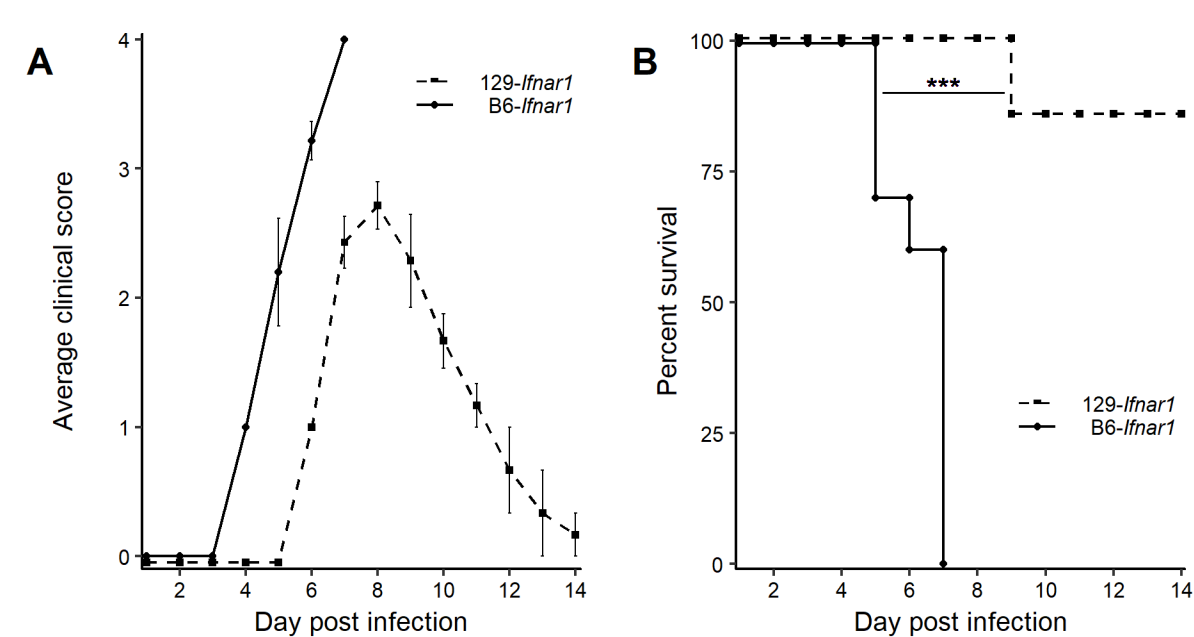1064   black, dashed red and plain red lines, respectively. No genome location reached the p = 0.05

1065   threshold.

1066   **FIG 6** Genetic variations between CC strains control brain viral load and histological profile of

1067   infected mice. Four to five mice of 129-*Ifnar1* and three selected CC strains were infected IP

1068   with 10^7 FFUs of ZIKV FG15 24hr after IP injection of 2 mg of MAR1-5A3 mAb. Top : Brain

1069   viral load was measured by RT-qPCR at day 6 p.i. (Wilcoxon, * : $p < 0.05$). Bottom :

1070   Representative brain sections of the same ZIKV FG15-infected mice, at day 6 p.i. (A-C) Lesions

1071   were clearly more severe for 129-*Ifnar1* mice (n=3), with subacute leptomeningo-encephalitis

1072   (*i.e.* infiltration of perivascular spaces and leptomeninges by lymphocytes, plasma cells and

1073   macrophages; arrows) and (D-E) activation of microglial cells with microglial nodules

1074   (arrowheads). (F-G) CC001 mice (n=5) displayed no significant histological lesions in the brain

1075   with normal resting (non-activated) microglial cells (H-I). Only very rare small clusters of

1076   activated microglial cells were detected (data not shown). By contrast, CC005 mice (n=5)

1077   displayed moderate inflammatory lesions characterized by (J-K) perivascular cuffing (arrow;

1078   n=2), (L-M) activation of microglial cells (hyperplasia and thickening of cell processes) and

1079   microglial nodules (arrowheads; n=5). CC071 mice (n=4) also displayed inflammatory lesions

1080   but with intermediate severity: (N-O) almost no lesions in HE but (P-Q) activation of microglial

1081   cells and microglial nodules (arrowhead). A, B, C, F, G, J, K, N, O : HE staining; D, E, H, I, L,

1082   M, P, Q : anti-Iba1 immunohistochemistry.

1083   **FIG 7** Intracranial ZIKV FG15 infection results in strain-dependent viral load and brain

1084   histological lesions. Mice of 129-*Ifnar1* and three selected CC strains (3-5 mice per strain) were

1085   infected IC with 10^5 FFUs of ZIKV FG15 in the absence of prior anti-IFNAR treatment. Top:

1086   CC005 and CC071 mice show significantly higher brain viral load at day 6 p.i. than CC001 mice

1087   (Wilcoxon, ** : p < 0.01). Bottom : After intracranial inoculation, lesion profiles were clearly

1088   different from those observed after IP inoculation. (A-C) 129-*Ifnar1* mice (n=4), still displayed

1089   marked subacute leptomeningo-encephalitis (arrow: leptomeningitis) and (D-E) activation of

1090   microglial cells. Two of the 5 CC001 mice displayed no significant histological lesions with

1091   normal resting microglial cells, while the other three displayed (J-K) minimal lesions with

1092   gliosis, and (H-I) rare small clusters of activated microglial cells. In this experimental model,

1093   CC005 mice displayed heterogeneous lesion profiles with either (i) suspected meningitis and (J-

1094   K) gliosis (n=4/5), or (ii) moderate leptomeningo-encephalitis (n=1/5). (L-M) Activation of

1095   microglial cells (arrowhead), with variable severity, was detected in all animals (n=5/5).

1096   Strikingly, (N-P) all CC071 mice (n=5/5) displayed marked leptomeningo-encephalitis (arrow:

1097   leptomeningitis) with (Q-R) strong activation of microglial cells. A, B, C, F, G, J, K, N, O, P :

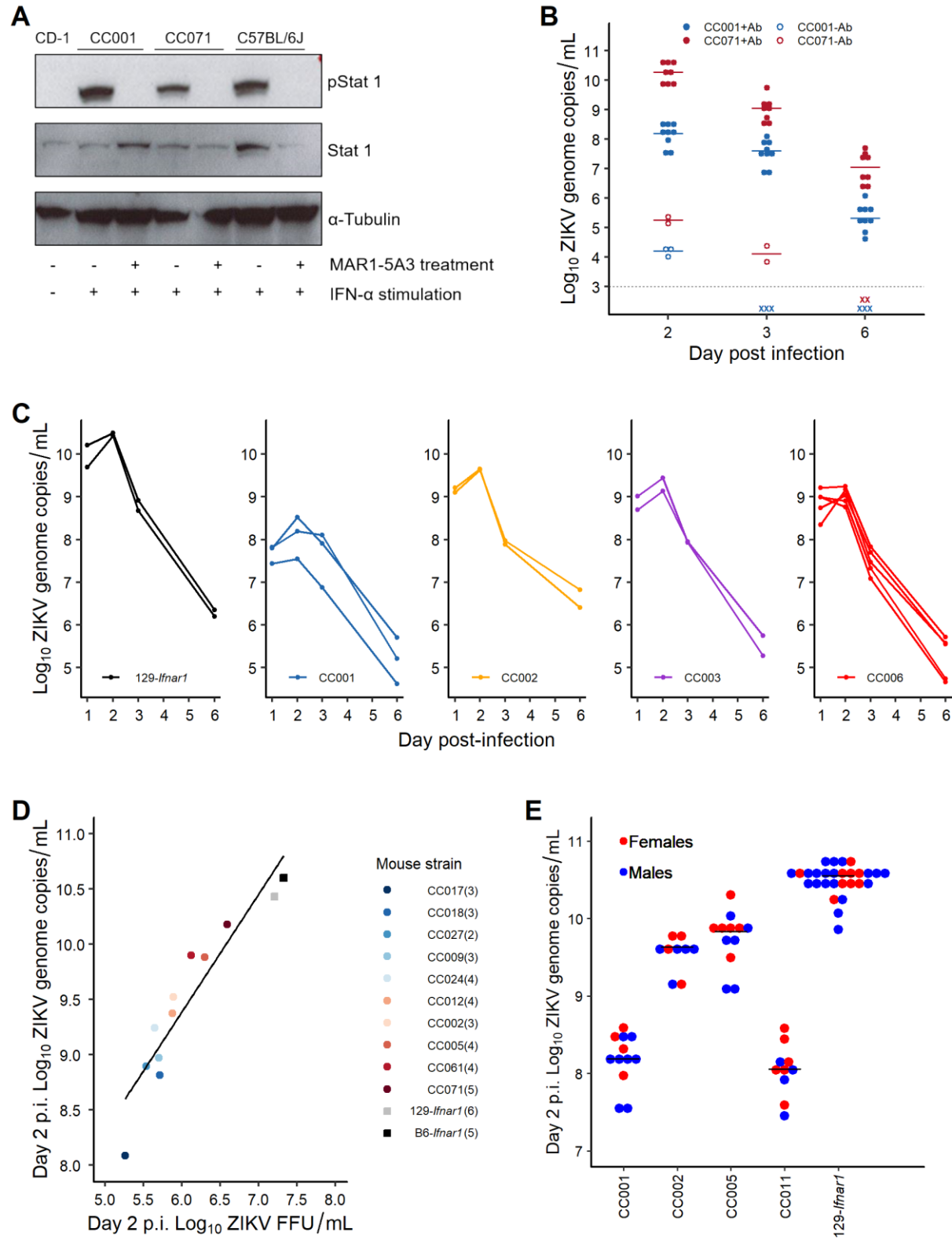1098   HE staining; D, E, H, I, L, M, Q, R : anti-Iba1 immunohistochemistry.

1099   **FIG 8** *In vivo* susceptibility to ZIKV FG15 in CC071 correlates with increased viral replication

1100   *in vitro* compared with CC001. Mouse cells were infected with ZIKV FG15 at MOI 5. ZIKV

1101   titer in the supernatant was quantified by focus-forming assay at 24, 48 and 72 hours p.i. (A)

1102   MEFs derived from CC001 (blue) and CC071 (red) embryos. Mean +/- SEM from 3 biological

1103   replicates. At 48h and 72 h p.i., CC071 MEFs produced significantly higher virus titers. (B)

1104   Macrophages isolated from peritoneal lavage. Mean +/- SEM from 2 replicates. CC071

1105   macrophages produced significantly higher virus titers at the three time points. (C) Neurons from

1106   fetal brain dissected at day 16.5 of gestation and cultured for 12 days before infection. Mean +/-

1107   SEM from 2 replicates. CC071 neurons produced significantly higher virus titers at 72 h p.i. (t

1108   tests; * p < 0.05, ** p < 0.01, *** p < 0.001).

1109   **FIGURES**

1110

1111
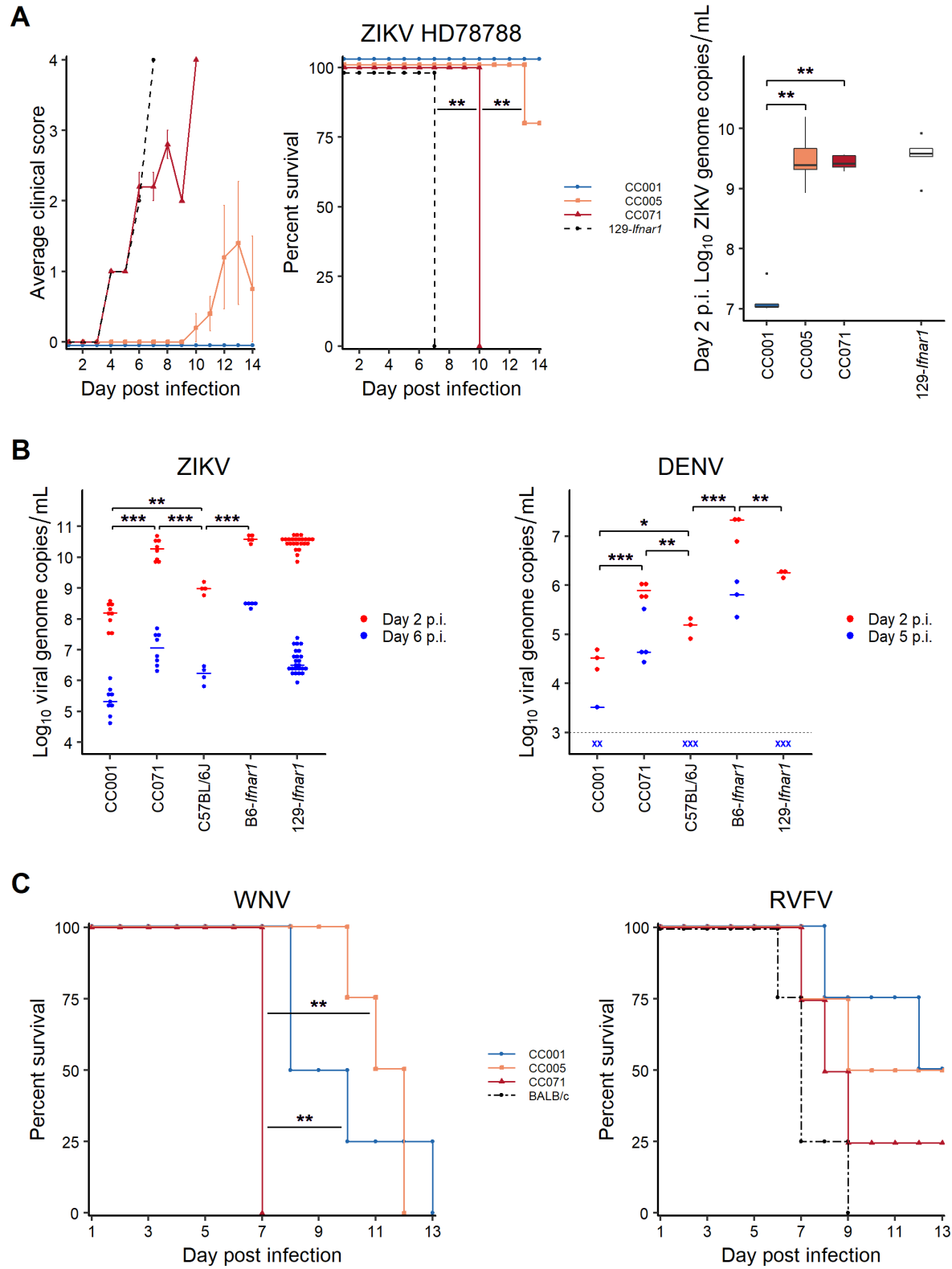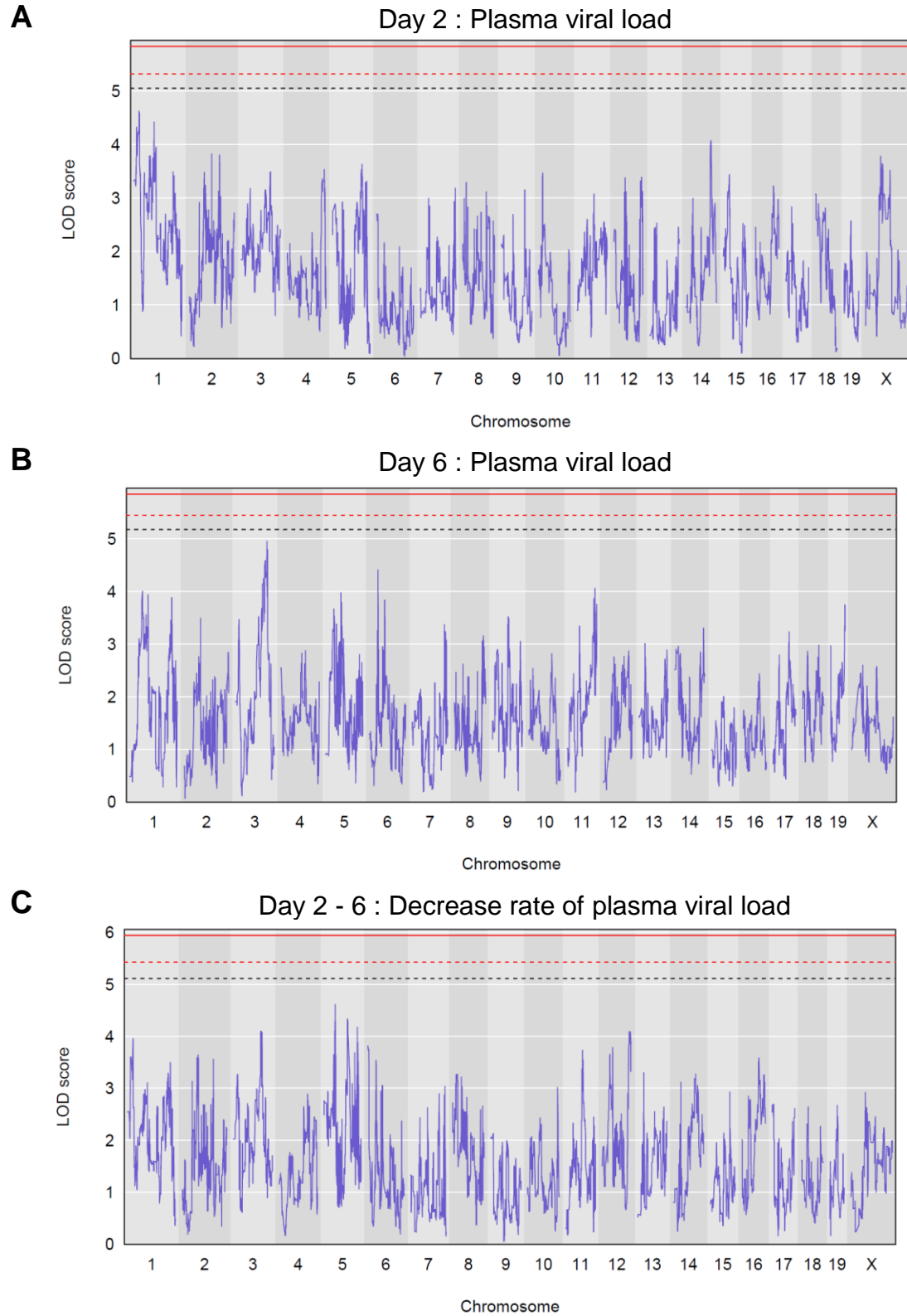1112   **Figure 1.**
1113

1114
1115 **Figure 2.**
1116

53

Figure 3.

Figure 4.

A

Day 2 : Plasma viral load

B

Day 6 : Plasma viral load

C

Day 2 - 6 : Decrease rate of plasma viral load

1123 **Figure 5.**

1124

56

1125

1126
1127 **Figure 6.**
1128

1129

1130
1131 **Figure 7.**
1132

58

A Embryonic fibroblasts

B Peritoneal macrophages

C Primary neurons

1133
1134 **Figure 8.**
1135
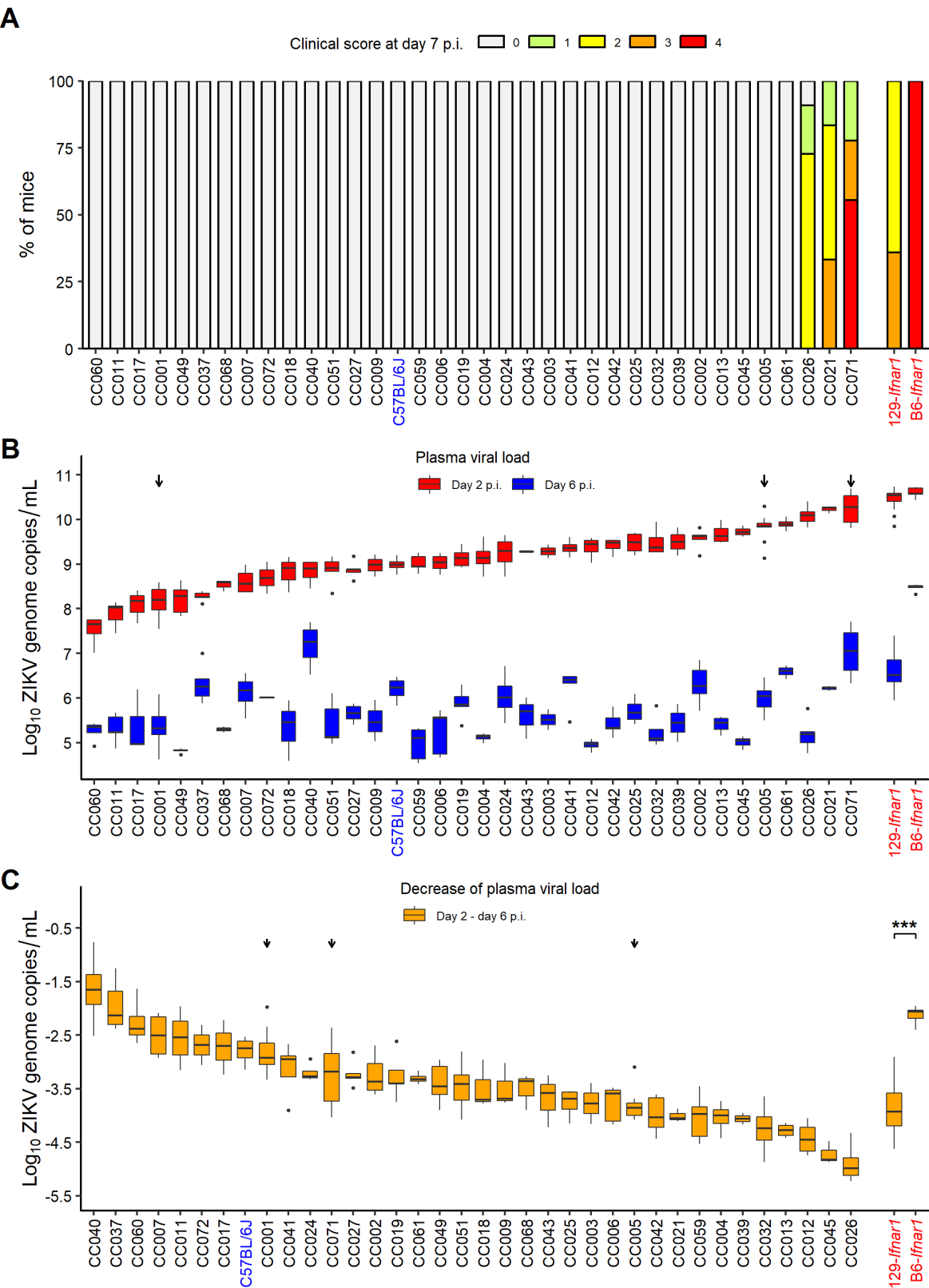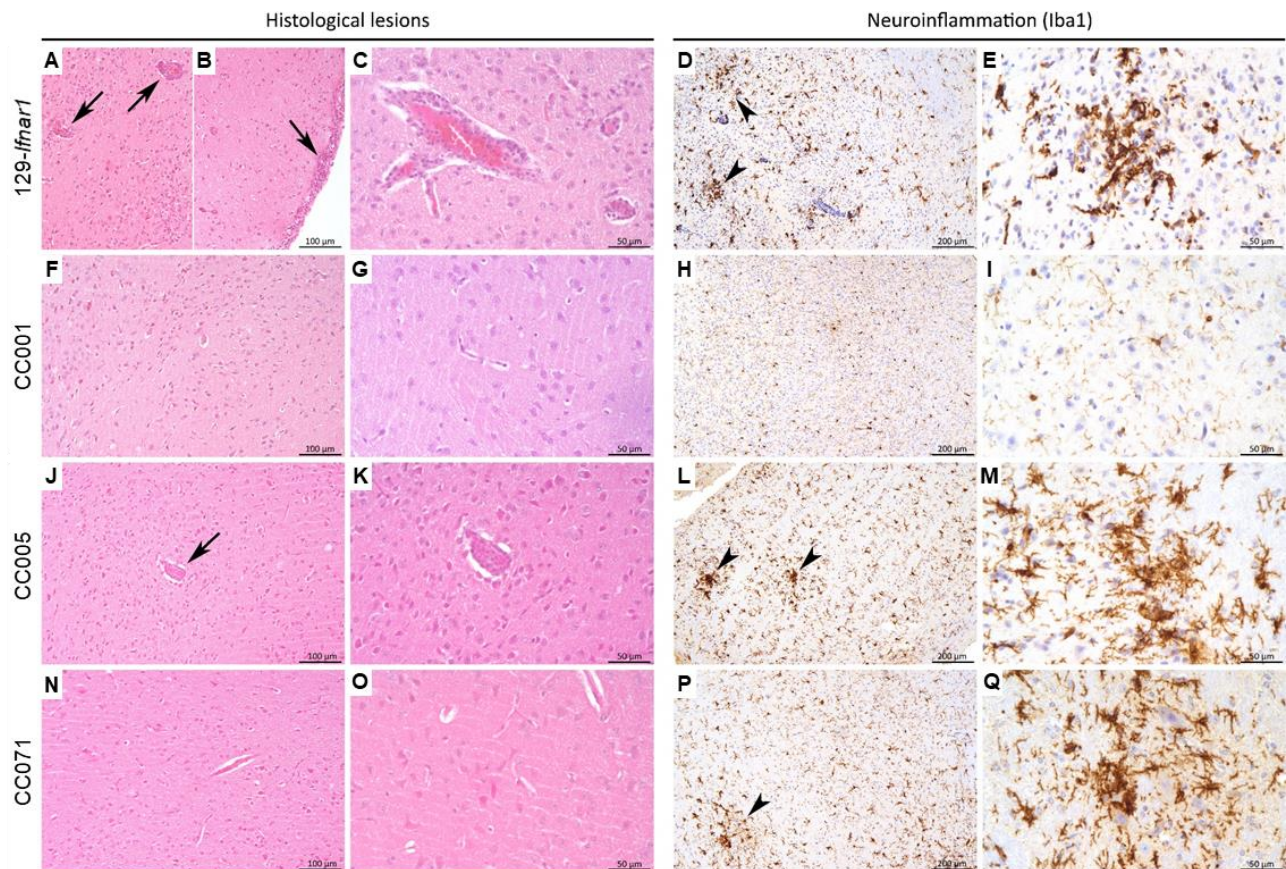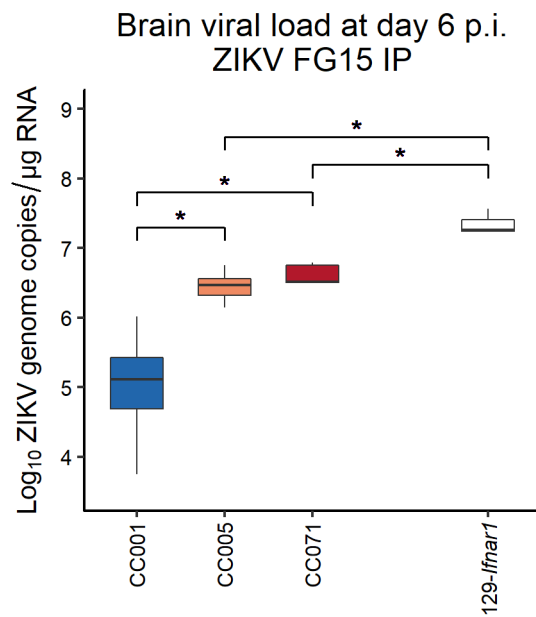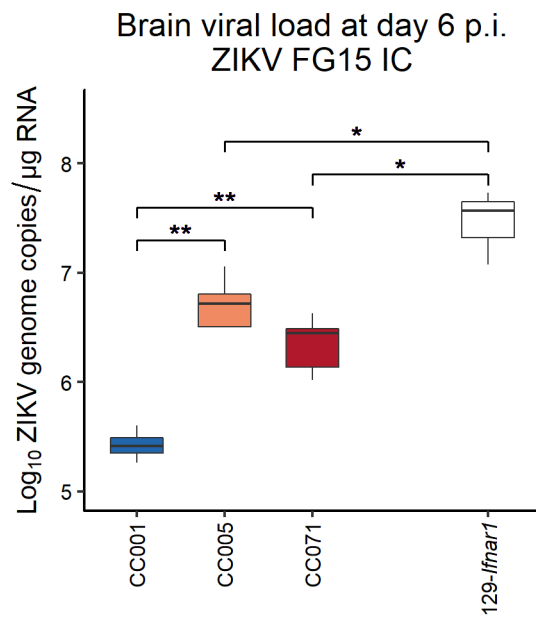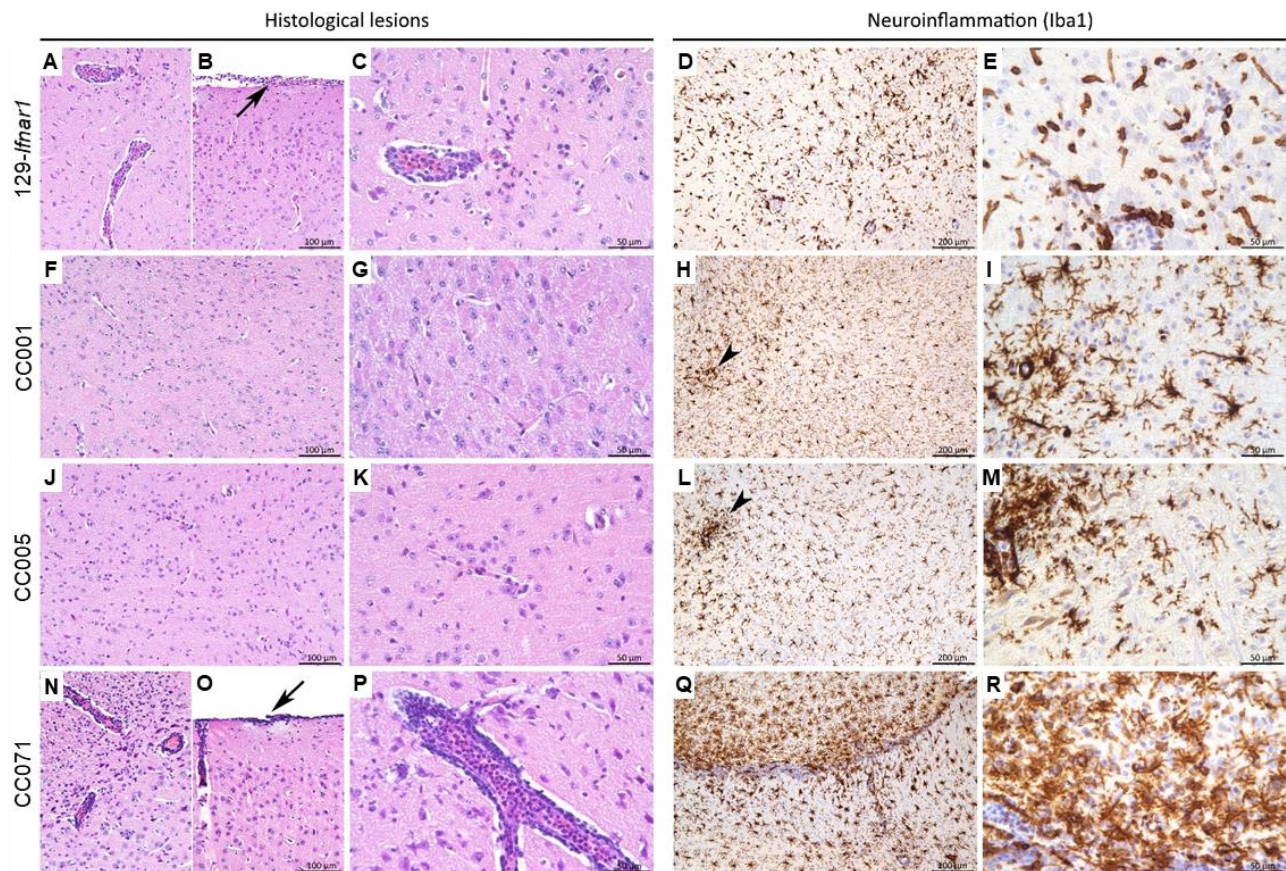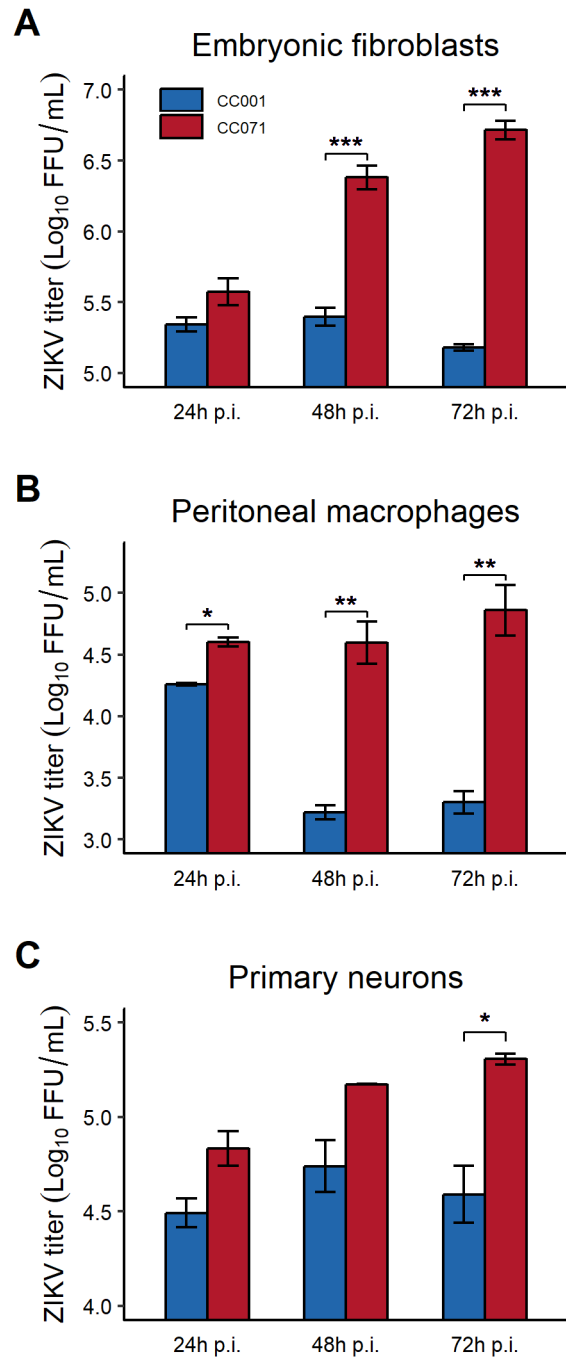
	CC001	CC005	CC071	129-*Ifnar1*
Symptoms	−	−	✚	✚
Mortality	0%	0%	78%	12.5%
Peak plasma viral load	+	✚	✚	✚
Rate of decrease of plasma viral load	↘	↓	↘	↓
Brain viral load (systemic infection)	+	✚	✚	✚
Brain pathology (systemic infection)	−	✚	+	✚
Brain viral load (intracerebral infection)	+	✚	✚	✚
Brain pathology (intracerebral infection)	✚	✚	✚	✚
Viral replication in vitro (24-72 hours)	↘	-	↗	-

Table 1. Summary of the main features of ZIKV infection in mAb-treated CC strains and 129-*Ifnar1* mice.